ABSTRACT

ZENG, KAIYUE. Uncertainty Analysis Framework for the Multi-Physics Light Water Reactor Simulation. (Under the direction of Jason Hou.)

In recent years, the demand to provide best estimate predictions with confidence bounds is increasing for the nuclear reactor performance and safety analysis. As a result, the best-estimate plus uncertainty method (BEPU) has been approved by US NRC as an alternative approach to the conventional conservative methods for nuclear reactor safety evaluation. Input uncertainties from multi-physics domains will be considered, including neutron-kinetic parameters (NK), fuel modeling (FM) and thermal-hydraulics (TH) modeling parameters. The goal of this work is to develop a framework for consistent uncertainty analysis of light water reactor modeling, with special consideration for the correlations between multi-physics input parameters.

In current BEPU approaches, the uncertain input parameters from different physics domains were considered independent from each other and so were their impact on the uncertainty of system responses. The consistent uncertainty propagation remains a challenging work and the impact of correlations of input parameters therefore needs to be quantified. This independent uncertainty propagation methodologies can introduce bias because the multi-physics input uncertainties may originate from the same fundamental source and thus be correlated with each other. For example, the uncertainties of fuel composition and enrichment have impacts on both assembly few-group constants (NK) and fuel thermal conductivity (FM). The uncertainty of core total power has impacts on both thermal-hydraulics (TH) calculation and the determination of gap conductance (FM) through the fuel expansion and thus gap size. The manufacturing uncertainties of fuel pellet radius, gap thickness, and cladding thickness have influences on NK parameters through the generation of few-group constants, on TH calculations through the determination of hydraulic diameter, and on the FM calculation through the modeling of gap conductance.

In this work, a consistent uncertainty analysis methodology is proposed to represent the correlations between input parameters involve the usage of the global variance-covariance matrix (VCM) covering the NK few-group constants, FM and TH parameters. The sampling approach is used in constructing the global VCM. A number of samples are generated by independently sample fundamental input uncertainties (e.g. the fuel-cladding gap size), and samples of input parameters from three different physics domains can be obtained by performing lattice calculations, fuel modeling or thermal-hydraulics modeling. Each sample which combines input parameters from NK, FM and TH domains is consistent as they can be corresponded into the same sample of fuel-cladding gap size. A global VCM covering the input parameters from three different physics domains can then be generated from these consistent samples. The consistent uncertainty input parameters can be generated with sampling approach through Cholesky decomposition of the global VCM and Latin Hypercube Sampling method, and passed into the core multi-physics simulations. Therefore, the proposed framework can be incorporated into the conventional two-step light water reactor simulations for uncertainty analysis purposes.

The proposed method is implemented into a Pressurized Water Reactor (PWR) mini-core problem and large scale core problem for demonstration. The uncertainties of multiple output responses including the steady state core keff and power distribution, the time evolution of reactivity, core transient power, and peak fuel temperatures are computed. The impact of taking into account the correlations between parameters from different physics domains is evaluated. The results show that by considering the correlations the core responses uncertainty and 95% percentile decreases. This provides more safety margins and highlights the importance of correlations in multiphysics core calculations.

© Copyright 2020 by Kaiyue Zeng

All Rights Reserved

Uncertainty Analysis Framework for the Multi-Physics Light Water Reactor Simulation

by
Kaiyue Zeng

A dissertation submitted to the Graduate Faculty of
North Carolina State University
in partial fulfillment of the
requirements for the Degree of
Doctor of Philosophy

Nuclear Engineering

Raleigh, North Carolina

2020

APPROVED BY:

Kostadin N. Ivanov	Maria Avramova
Ralph C. Smith	Jason Hou Chair of Advisory Committee

DEDICATION

To my dear family and friends.

BIOGRAPHY

The author was born in China and graduated from Huazhong University of Science and Technology with a bachelor's degree in Nuclear Engineering in 2014. He has been a graduate student in department of Nuclear Engineering, North Carolina State University since August 2014. He joined Dr. Igor Bolotnov's group from 2014 to 2016 and obtained his master's degree. He then moved to Dr. Jason Hou's group and focuses on sensitivity and uncertainty analysis of reactor modeling.

ACKNOWLEDGEMENTS

First of all, I would like to express my sincerest appreciation to my advisor Dr. Jason Hou for his support and guidance during my Ph.D. career and his advice for conducting this research work. I would like to thank my committee members (Dr. Ivanov, Dr. Avramova, Dr. Smith, Dr. Jessee and Dr. Swiler) for their guidance and effort in supporting this study. I am also grateful to my colleagues in my research group who helped me a lot in completing this study.

TABLE OF CONTENTS

LIST OF TABLES . . . . . **vii**

LIST OF FIGURES . . . . . **viii**

Chapter 1 INTRODUCTION **1**
1.1 Best Estimated Plus Uncertainty Approach 1
1.2 Thesis Outline 9

Chapter 2 DEVELOPMENT OF THE CONSISTENT UNCERTAINTY PROPAGATION METHODOLOGY **10**
2.1 Consistent Uncertainty Propagation for Two-Step Core Simulation 12
2.2 Quantification of Confidence Intervals 15

Chapter 3 INVESTIGATION OF CORRELATIONS BETWEEN DIFFERENT PHYSICS DOMAINS **18**
3.1 Multi-physics Model of the PWR Mini-Core 19
3.2 Events Description 23
3.3 Verification of VCM Generation 23
3.4 Correlation of Input Parameters 29
3.4.1 NK-TH Correlation Study 32
3.4.2 NK-FM Correlation Study 34
3.4.3 NK-FM-TH Correlation Study 36
3.5 Summary 37

Chapter 4 CONSISTENT UNCERTAINTY ANALYSIS OF THE TMI-1 REACTOR CORE 38
4.1 TMI-1 Reactor Core 39
4.2 Numerical Test Cases 39
4.3 Multi-Physics PWR Core Model 41
4.4 Uncertainty Analysis of PWR Steady State Simulation 42
4.5 Uncertainty Analysis of PWR Transient Simulation 50
4.6 Uncertainty Analysis of PWR Cycle Depletion Simulation 56
4.7 Summary 58

Chapter 5 CONCLUSIONS AND FUTURE WORK **59**
5.1 Conclusions 59
5.2 Future Work 61

BIBLIOGRAPHY **63**

APPENDIX **66**
Appendix A IMPACT OF SPATIAL COUPLING SCHEMES AND PERTRUBATION OPTIONS ON UNCERTAINTY QUANTIFICATION OF PWR CORE SIMULATION 67

A.1 Coupling Schemes 69
A.2 Input Uncertainties 69
A.3 Impact of Spatial Coupling Schemes on Core Uncertainty Quantification 72

LIST OF TABLES

Table 3.1 Summary of core output responses comparing case 1 and case 2. . . 30
Table 3.2 Summary of the geometrical manufacturing uncertainties considered for PWR mini-core problem. 30
Table 3.3 Impact of the correlated and uncorrelated input uncertainties on core outputs by taking into account NK-TH correlations. 35
Table 3.4 Impact of the correlated and uncorrelated input uncertainties on core outputs by taken into account NK-FM correlations. 36
Table 3.5 Impact of the correlated and uncorrelated input uncertainties on core outputs by taken into account NK-TH correlations. 37

Table 4.1 Core Physics Parameters at Nominal State. 43
Table 4.2 Summary of the geometrical manufacturing uncertainties considered for TMI-1 large-scale core problem. 44
Table 4.3 Summary of the geometrical manufacturing uncertainties considered for TMI-1 Reactor Core Steady State Simulation. 46
Table 4.4 A^2 and corresponding $p-values$ for power peaking factors at various core states. 47
Table 4.5 Summary of uncertainty quantification on selected core parameters at steady state simulations (numbers given in mean ± relative standard deviation). 51
Table 4.6 Summary of uncertainty quantification for TMI-1 REA transient simulations (numbers given in mean + [95th/95% tolerance limit - mean]). 55

Table A.1 Summary of the geometrical manufacturing uncertainties considered for TMI-1 large-scale core problem. 71

LIST OF FIGURES

Figure 1.1 Concept of BEPU approach and the benefit of BEPU analysis compared to conservative analysis [9]. 3
Figure 1.2 Multi-physics multi-scale uncertainty quantification, with uncertainty originated from boundary condition (B.C.), modeling assumption, geometrical uncertainty and data uncertainty. 4
Figure 1.3 Strategy for uncertainty propagation from single physics to multi-physics simulations [12]. 6
Figure 1.4 Input uncertain parameters together with their fundamental sources of uncertainty. 8

Figure 2.1 Structure of the global variance-covariance matrix (VCM). 11
Figure 2.2 PWR core consistent uncertainty quantification with the stochastic sampling method. 12
Figure 2.3 Confidence intervals corresponding to different sample size. 17

Figure 3.1 PWR mini-core radial layout. 20
Figure 3.2 Conventional two-step LWR simulation approach. 21
Figure 3.3 Heat conduction (HtStr) and thermal-hydraulics (TH) model, axial NK-FM-TH mapping. 21
Figure 3.4 Cross section parameterization for fuel assemblies with control rod. 22
Figure 3.5 Correlation matrix of few-group constants. 24
Figure 3.6 Correlation matrix for PWR mini-core problem. 25
Figure 3.7 Distributions of original data (left), inverse transform sampling of CDF (mid.), and comparison of the distributions between original data and re-sampling data. 27
Figure 3.8 Running sample mean and uncertainty of the critical boron concentration at case 1 (left) and case 2 (right). 27
Figure 3.9 Radial power distributions with associated uncertainties corresponding to case 1 (left) and case 2 (right). 28
Figure 3.10 Time evolution of core reactivity, total core power, and peak fuel temperatures under case 1 (left) and case 2 (right) configurations. . 29
Figure 3.11 Time evolution of core reactivity, total core power, and peak fuel temperatures under case 1 (left) and case 2 (right) configurations. . 33
Figure 3.12 Running sample mean and uncertainty of the critical boron concentration at correlated case (left) and uncorrelated case (right). 33
Figure 3.13 Radial power distributions with associated uncertainties corresponding at correlated case (left) and uncorrelated case (right). 34
Figure 3.14 Time evolution of peak fuel temperatures under at correlated case (left) and uncorrelated case (right) configurations. 34
Figure 3.15 Correlation between few-group constants and gap conductance (NK-FM correlation). 35

Figure 4.1 TMI-1 quarter core configuration. 40
Figure 4.2 One Dimensional Channel model: TRACE TH, HTSTR models, and TH-HTSTR-NK mapping. 42
Figure 4.3 Correlation matrix of few-group constants, H_{gap}, D_h, A_x and P_w. . . 43
Figure 4.4 Running mean k_{eff} for HFP at BOC. 45
Figure 4.5 Running mean k_{eff} for HFP at EOC. 45
Figure 4.6 Frequency histogram of core key axial power peaking factors at HFP EOC state. 47
Figure 4.7 Core axial power under HFP BOC and HFP EOC steady states. 48
Figure 4.8 Radial power distribution at BOC 49
Figure 4.9 Radial power distribution at EOC. 50
Figure 4.10 Core net reactivity during transient, initiated from HFP at BOC. . . . 52
Figure 4.11 Core net reactivity during transient, initiated from HFP at EOC. . . . 53
Figure 4.12 Normalized core power during transient, initiated from critical HFP at BOC. 53
Figure 4.13 Normalized core power during transient, initiated from critical HFP at EOC. 54
Figure 4.14 Peak fuel temperature during transient, initiated from HFP at BOC. 54
Figure 4.15 Peak fuel temperature during transient, initiated from HFP at EOC. 55
Figure 4.16 Core Burnup Distribution and Relative Error at EOC. 56
Figure 4.17 Burnups at EOC with Associated Uncertainties with consideration of NK-FM-TH correlations. 57
Figure 4.18 Burnups at EOC with Associated Uncertainties without consideration of NK-FM-TH correlations. 57

Figure A.1 Axial TH-HTSTR-NK Mapping(a), 1-D Channel Model (b), 3-D Cartesian Model (c). 70
Figure A.2 PWR Core Uncertainty Quantification with Stochastic Sampling Method. 72

CHAPTER

1

INTRODUCTION

1.1 Best Estimated Plus Uncertainty Approach

The computational nuclear reactor safety analysis was initially performed with the conservative methods, which have been finalized with the United States Nuclear Regulatory Commission as 10 CFR 50.46 in 1974 [1]. It established the safety limits for peak cladding temperature, maximum cladding oxidation, maximum hydrogen generation, etc. This conservative approach ensures sufficient safety margins. However, it also tends to produce excessive conservatism due to the conservative assumption and thus makes the core design not economical. The best estimated plus uncertainty method (BEPU) originated since 1988 when U.S.NRC revised the rules and accepted BEPU as an alternative approach to the conventional conservative method [2], [3], [4], [5], [6], [7]. Since then the nuclear community

has grown interests in the application of best estimate plus uncertainty methodology in nuclear engineering problem. A series of workshops and benchmarks were launched by OECD NEA.

Figure 1.1 illustrates the benefit of using BEPU method compared to the traditional conservative method [8]. The safety limits such as peak cladding temperature were set up in a way that exceeding the limit would result in damage of the safety barrier. The actual margin could be computed as the distance between the real value and the safety limit. The acceptance criterion for reactor licensing purpose is usually determine by assigning some margins to the safety limits. In the conservative approach, the calculated conservative value is calculated following the guideline proposed in [9] by assigning margins to input parameters and assumptions. Therefore, the calculated conservative value is close to the acceptance criterion. The BEPU approach, calculates a more realistic prediction, and provides associated uncertainty bounds. The distance of the 95th upper bound of uncertainty to the acceptance criterion is then taken as the BEPU margin. The BEPU approach is believed to yield larger margins compared to the conservative margin because no conservative hypotheses were made during the calculation, and therefore produce a more economic reactor design.

In order to establish the accuracy and confidence for best estimate codes, the uncertainty in reactor modelling must be quantified. In recent years, the demand to provide best estimate predictions with confidence bounds is increasing in the areas of nuclear research, industry, safety and regulation [10]. The uncertainty analysis has been regarded as a significant part in nuclear reactor design and analysis. Consequently, the Organization for Economic Cooperation and Development (OECD) Nuclear Energy Agency (NEA) has been developing an international benchmark for the uncertainty analysis in modelling of light water reactors (LWR-UAM) since 2006 for the examination of uncertainty quantification and propagation methodologies for various modelling and simulation code systems [11]. The objective of this benchmark is to provide an international framework to drive

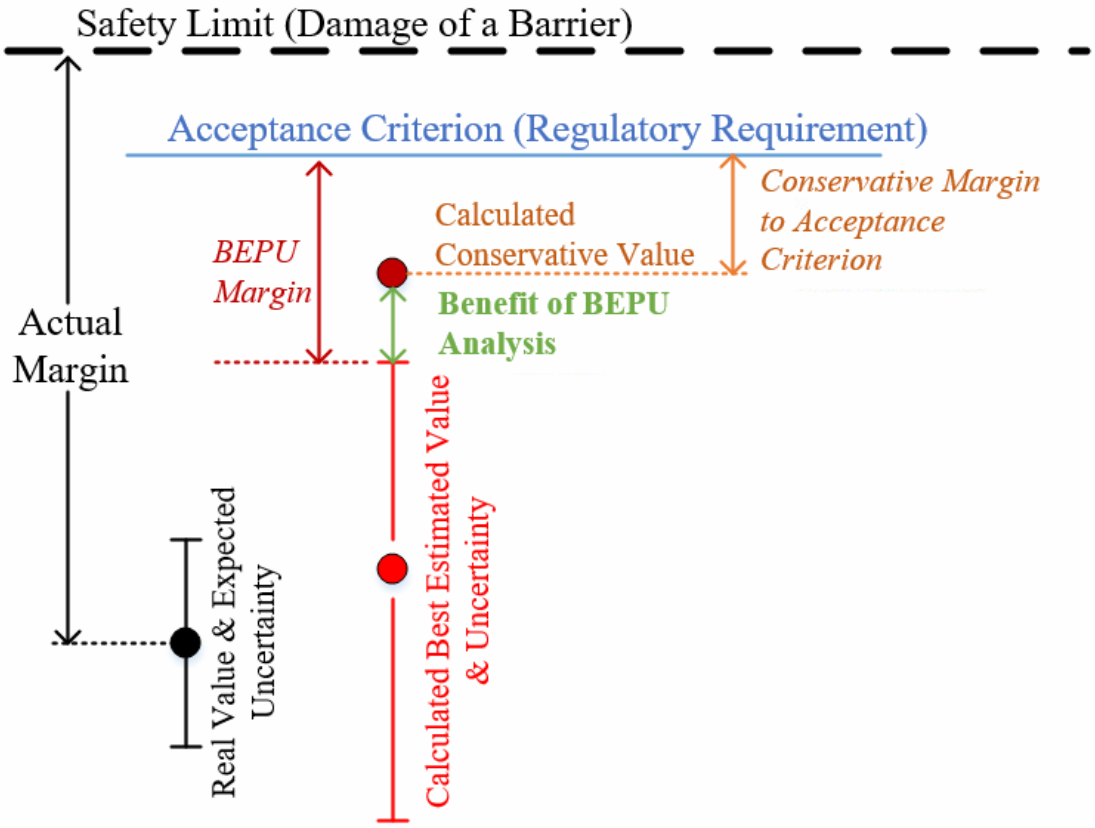

Figure 1.1 Concept of BEPU approach and the benefit of BEPU analysis compared to conservative analysis [9].

forward the development, assessment, and integration of the comprehensive uncertainty quantification methods in best estimate multi-physics coupled simulations of LWRs during normal and transient conditions [12].

As shown in Figure 1.2, a series of reference systems and scenarios are defined with complete sets of input specifications and experimental data. The benchmark is being carried out in three phases with increasing modelling complexity, while each phase are further subdivided into multiple exercises [12]:

- Phase I (neutronics phase):
  - Exercise I-1 (Cell physics): Calculation of the multi-group microscopic cross-sections with associated uncertainties.

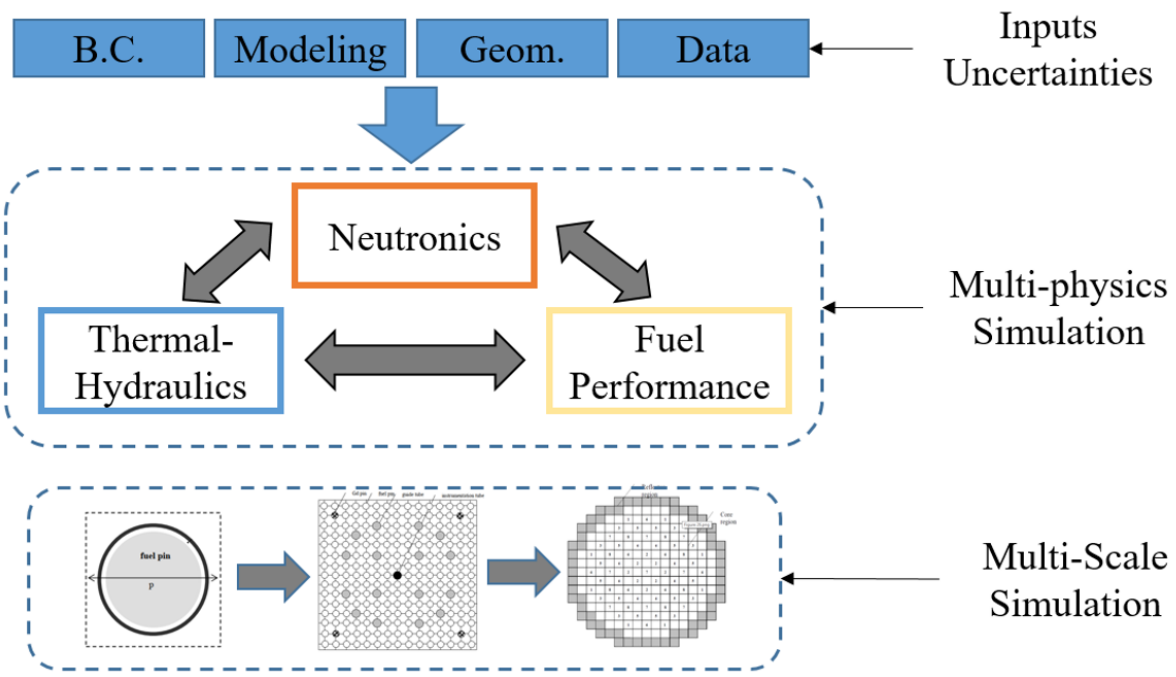

Figure 1.2 Multi-physics multi-scale uncertainty quantification, with uncertainty originated from boundary condition (B.C.), modeling assumption, geometrical uncertainty and data uncertainty.

  - Exercise I-2 (Lattice physics): Calculation of the few-group macroscopic cross-sections with associated uncertainties.
  - Exercise I-3 (Core physics): Core steady state standalone neutronics calculations with associated uncertainties.

- Phase II (core phase):
  - Exercise II-1 (Fuel modelling): Modelling of fuel thermal properties with associated uncertainties.
  - Exercise II-2 (Time dependent neutronics): Neutron kinetics and fuel depletion standalone performance with associated uncertainties.
  - Exercise II-3 (Bundle thermal-hydraulics): Thermal-hydraulics fuel bundle performance with associated uncertainties.

- Phase III (system phase):

- Exercise III-1 (Core multi-physics): Couple neutronics/thermal-hydraulics core simulation with associated uncertainties. This exercise includes coupled steady state, coupled depletion, and transient simulations with propagation of uncertainties from multi-physics domains including neutronics, fuel modelling and thermal-hydraulics.
- Exercise III-2 (System thermal-hydraulics): Calculation of the thermal-hydraulics system performance with associated uncertainties.
- Exercise III-3 (Coupled core-system): Coupled neutronics kinetics thermal-hydraulic core/thermal-hydraulic system performance.
- Exercise III-4: Comparison of best estimate plus uncertainty (BEPU) vs. Conservative Calculations.

The current approach for uncertainty propagation from three single physics domains to multi-physics uncertainty quantification is depicted in Figure 1.3. The uncertainties of different input parameters are calculated with considering the modelling uncertainties, geometry uncertainties, uncertainties related to boundary condition and measurement data. The output parameters from single physics are then passed into multi-physics simulation with nominal value and associated uncertainty bounds.

Currently, a variety of studies about uncertainty quantification of the LWR-UAM Benchmark have been performed. Direct perturbation and stochastic sampling methods were developed at Paul Scherrer Institute and implemented in CASMO-5MX and MCNPX, respectively, to quantify the uncertainty of UAM benchmark Exercise I-1 (cell physics) and I-2 (lattice physics). Uncertainties calculated from different methods agree with each other quite well, and the isotopes which contributed more to the outputs uncertainty were selected out and reported [13]. The TMI-1 core standalone neutronic simulation (Exercise I-3) was performed in [14], and the core multiplication factor, power peaking factors were calculated with associated uncertainties. Many other works related to the quantification

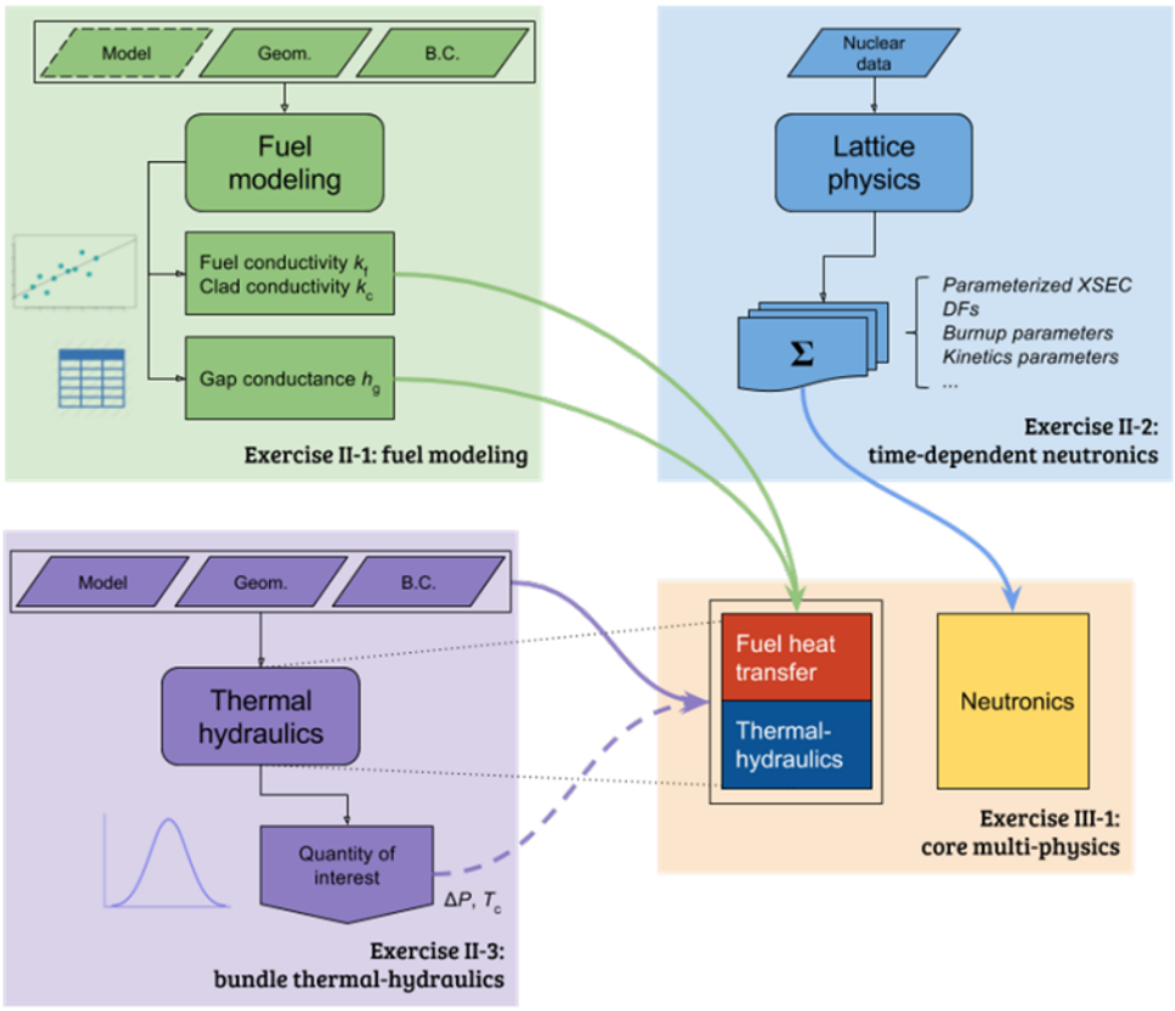

Figure 1.3 Strategy for uncertainty propagation from single physics to multi-physics simulations [12].

of the uncertainties in Phase I have been summarized in [15]. Three reactor systems including the Peach Bottom Unit 2 BWR, Three Mile Island Unit 1 PWR, and VVER-1000 Kozloduy-6/Kalinin-3 have been studied. The methods of rigorous nuclear data uncertainty propagation have been widely investigated in multi-scale simulations including pin cell, assembly lattice and standalone core neutronics.

Many research works have been conducted for Phase II. The fuel modelling uncertainties were evaluated in Exercise II-1 by considering the input uncertainties from boundary conditions and fuel rod geometry as presented in [16]. Uncertainty quantification of the

six-group kinetic parameters (Exercise II-2) were investigated and reported in [17] using a sampling-based method, and the capability of quantifying uncertainty from delayed neutrons data would be available in the future release of SCALE code package. The uncertainty quantification of TMI-1 subchannel thermal-hydraulics was investigated in [16]. A sensitivity analysis was performed to eliminate input parameters that have minimal influence on the quantities of interest, and the final thermal-hydraulic fuel bundle performance were reported with associated uncertainties (Exercise II-3). Various output quantities from multiple physics domains have been evaluated in Phase II and are treated as input uncertainties for reactor core multi-physics simulation (Exercise III-1), as discussed in [18]. Commissariat à l'Energie Atomique (CEA) studied a PWR mini-core, and performed uncertainty analysis in a control rod ejection accident. Separate studies with different level of multi-physics coupling were first conducted, and the input uncertainties were finally propagated to the core transient through the APOLLO3-FLICA4-ALCYONE coupling code framework [19].

The uncertainty quantification and propagation in Exercise III-1 are an on-going topics of research [14], [20]. For Exercise III-1, the input uncertainties considered for multi-physics core simulations are grouped into three categories: fuel modelling uncertainties from Exercise II-1, netronics uncertainties from Exercise II-2, and thermal-hydraulics uncertainties from Exercise II-3. Previous studies related to LWR core multi-physics uncertainty propagation treats input uncertainties from multi-physics domains as independent parameters. However, this assumption may introduce error/bias because input parameters are correlated with each other due to the fact that their uncertainties may originate from the same source. Figure 1.4 illustrates the input uncertainties of three different physics domains. These uncertainties can be tracked back to common multiple fundamental sources. For example, the uncertainty of the fuel pellet size due to the fabrication inaccuracy will not only affect the material volume ratio during the cross section homogenization, which leads to uncertainty in few-group cross sections, but also impact the fuel thermal conductivity and gap conductance. The fuel composition, enrichment and density contributes to the

uncertainties of input parameters from neutronics and fuel modelling domains.

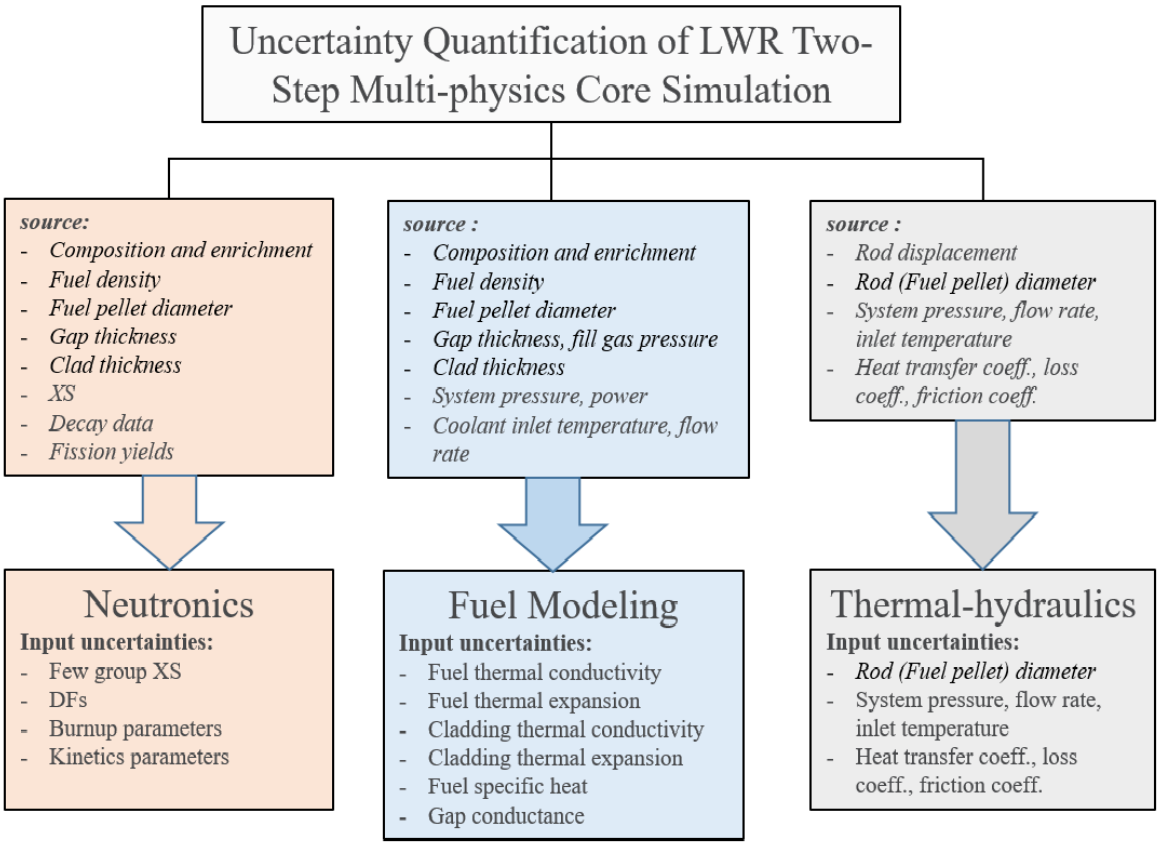

Figure 1.4 Input uncertain parameters together with their fundamental sources of uncertainty.

As a result, there is a need to propose an uncertainty analysis method for consistently propagating uncertainty in multi-physics LWR simulations. In this work we propose a framework that includes the following features:

1. it could be incorporated into the conventional light water reactor multi-physics simulation.

2. it should include uncertainties from three major physics domains.

3. the correlation of the input uncertainties should be propagated through multi-physics simulation in an consistent way, which means that the correlations of input parame-

ters must be quantified and propagated consistently.

4. it should be able to provide best-estimate predictions with uncertainty bounds and associated confidence levels.

1.2 Thesis Outline

In Chapter 2 a literature review of the statistical approach adopted for uncertainty analysis is performed. The Cholesky Decomposition is explained in detail. The methodology for multi-physics uncertainty propagation with consideration of the correlations between input uncertain parameters is presented in Chapter 2. The Anderson-Darling normality test is also described and the method of establishing the confidence intervals with certain confidence level is presented.

Chapter 3 focuses on the demonstration of the proposed consistent uncertainty propagation framework through the application of the method in a PWR mini-core problem. The multi-physics core steady state and control rod ejection transient are simulated and the output responses are evaluated with associated uncertainties. The impact of the correlations of input parameters on the uncertainties of core output responses is evaluated.

Chapter 4 presents the application of the framework on the Three Mile Island Unit # 1 (TMI-1) reactor core. The uncertainties of core output responses are evaluated by propagating input uncertainties with and without the consideration of correlations between input parameters. Three types of problems related to Exercise III-1 of the LWR-UAM benchmark are studied, namely steady state calculation, control rod ejection accident, and cycle depletion analysis. The core simulation results are reported with associated uncertain confidence bounds.

Finally, Chapter 5 summarizes the general observations of this work and some recommendations about what can be done in the future to enhance the proposed framework.

CHAPTER

2

DEVELOPMENT OF THE CONSISTENT UNCERTAINTY PROPAGATION METHODOLOGY

The approach for LWR simulation that is widely used in the industrial community is the two-step approach, which involves the generation of neutronic few-group constants as the first step, and the multi-physics core simulation as the second step. Code predictions are uncertain due to several sources of uncertainty, including neutron-kinetic (NK), fuel modeling (FM) and thermal-hydraulics (TH) parameters.

The goal of this study is to develop a methodology for consistent uncertainty propagation of the conventional two-step LWR core simulation. To quantify the impact of the

correlation between parameters from different physics domains on uncertainty analysis, a global variance-covariance matrix (VCM) needs to be constructed. As shown in Figure 2.1, the VCM consists of four regions. Region 1 represents the variance-covariance information of NK few-group constants, while region 2 corresponds to the TH or FM parameters. Region 3 and region 4 are symmetric and reflect the covariance between parameters from different physics domains. The VCM can be further sampled to generate correlated realizations of parameters, and the uncertainties of reactor core quantities of interest can be quantified using a stochastic sampling approach.

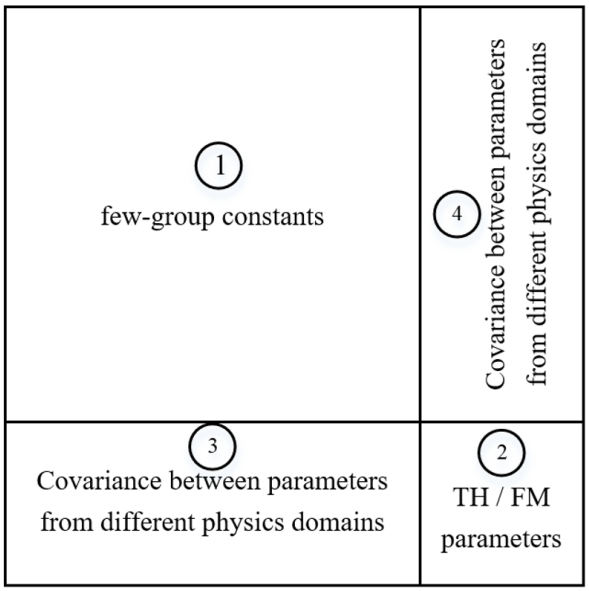

Figure 2.1 Structure of the global variance-covariance matrix (VCM).

This Chapter focuses on the development of the methodology for multi-physics uncertainty propagation with consideration of the correlations between multiphysics input uncertain parameters.The statistical approach for determination of the sample size and the condidence intervals estimation is also presented.

2.1 Consistent Uncertainty Propagation for Two-Step Core Simulation

The stochastic sampling method is used on the two stages of the reactor core simulation, namely, the transport lattice and nodal core calculations, to propagate the uncertainties from nuclear data, fuel modelling and thermal-hydraulic parameters to output responses [21]. The uncertain input variable vector X for nodal core simulation includes few-group constants Σ, fuel modeling parameters γ_f and thermal-hydraulic parameters γ_{th}, as shown in Eq. 2.1.

$$X = [\Sigma, \quad \gamma_f, \quad \gamma_{th}] \tag{2.1}$$

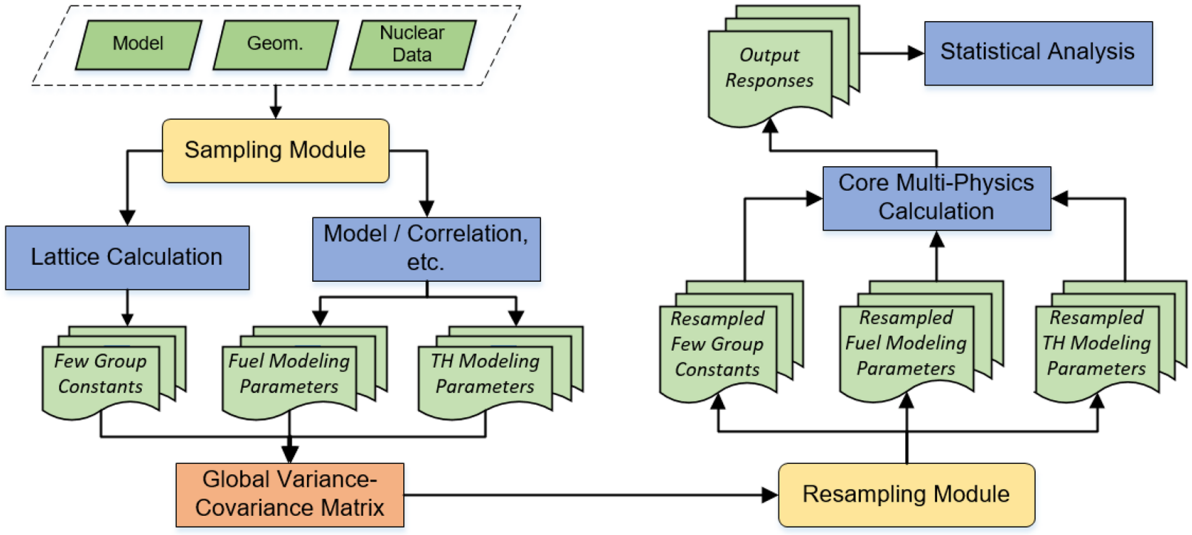

Figure 2.2 PWR core consistent uncertainty quantification with the stochastic sampling method.

In the sampling approach, X^k represents the various sets of variable realizations, while

k and K are the index and the total number of realizations, respectively.

$$X^k = [\Sigma^k, \quad \gamma_f^k, \quad \gamma_{th}^k]; \qquad k = 1, 2, ..., K \tag{2.2}$$

The correlations between input variables of $[\Sigma, \gamma_f, \gamma_{th}]$ can be evaluated, by tracing back the uncertainties into the same uncertain source as illustrated in Figure 1.4. As shown in Figure 2.2, the uncertainties of X can be traced back into original multi-group nuclear data σ, modeling and geometrical uncertainties ρ, whose correlation has been evaluated (e.g., nuclear data VCM) or can be reasonably assumed as independent variable (e.g. fuel pellet outer surface and cladding thickness). Since the correlations are well known, a direct sampling procedure can be performed for generating realizations. These realizations can then be passed into lattice physics code and other modelling tools to generate X^k.

With the abovementioned procedure, the consistency between different variables inside $[\Sigma, \gamma_f, \gamma_{th}]$ can be maintained. The correlation information is carried in various realizations of X^k. Based on these realizations a global VCM can be estimated:

$$C_x = \begin{pmatrix} Var(\Sigma) & Cov(\Sigma, \gamma_f) & Cov(\Sigma, \gamma_{th}) \\ Cov(\gamma_f, \Sigma) & Var(\gamma_f) & Cov(\gamma_{th}, \gamma_{th}) \\ Cov(\gamma_{th}, \gamma_f) & Cov(\gamma_{th}, \gamma_f) & Var(\gamma_{th}) \end{pmatrix} \tag{2.3}$$

where the diagonal terms are the variance and off-diagonal terms are covariances. By definition, the variance and covariance of variable x and y can be statistically estimated from a dataset of K random realizations as:

$$Var(x) = \frac{1}{K-1} \sum_{1}^{K} \left(x^k - \bar{x}\right)^2 \tag{2.4}$$

$$Cov(x) = \frac{1}{K-1} \sum_{1}^{K} \left(x^k - \bar{x}\right)\left(y^k - \bar{y}\right) \tag{2.5}$$

Once the global VCM is constructed, a sampling process can be performed to generate

the correlated realizations x^k. With x^k as input and the core multi-physics computational model, the reactor core output response R can be evaluated as a function of X as Eq. 2.7:

$$R = R(X) \tag{2.6}$$

$$R^k = R(X^k), \quad k = 0, 1, 2, ..., K \tag{2.7}$$

Once various core simulations are executed, the best-estimate core predictions and associated uncertainty of core output response R can be evaluated as the mean value and standard deviation.

Obviously, output responses R can be any response of interests such as core k_{eff}, peak temperature, etc. In order to estimate the uncertainty of R, all one needs to do is to perform a direct sampling of the global VCM and perform corresponding core multi-physics simulations. The correlated sampling process of the global VCM is achieved by first performing a Cholesky decomposition of C_X as Eq. 2.8:

$$C_x = L \cdot L^T \tag{2.8}$$

where, matrix L is a lower triangular matrix and L^T is the transpose of L. The correlated sample of X^k can then be computed as Eq. 2.9:

$$Y = \bar{X} + L \cdot Z \tag{2.9}$$

where $\bar{X}$ is a vector containing mean values, and vector Z is a random sample vector obtained by directly sampling a unit distribution (for example, a standard normal unite distribution $N(0,1)$). The obtained vector Y represents the correlated input space vector. Through mathematical derivation, it can be proved that the sampled random vector Y

follows the same distribution as $Y \quad N(\bar{X}, C_X)$:

$$E(Y) = E(\bar{X} + L \cdot Z) = E(\bar{X}) + E(L \cdot Z) = \bar{X} \tag{2.10}$$

$$\begin{aligned} Var(Y) & \\ &= E[(Y - E(Y))(Y - E(Y))^T] \\ &= E[(\bar{X} + L \cdot Z - \bar{X})(\bar{X} + L \cdot Z - \bar{X})^T] \\ &= E(L \cdot Z \cdot Z^T \cdot L^T) \\ &= L \cdot L^T \\ &= C_x \end{aligned} \tag{2.11}$$

To perform Cholesky decomposition successfully, the VCM should be positive definite and symmetric, which may not always practically the case. As a result, a procedure is performed to compute the eigenvalues of the matrix, and replace the negative ones with small positive value (10^{-10}), and then re-construct the VCM for the Cholesky decomposition.

2.2 Quantification of Confidence Intervals

The VCM is sampled with a size N and the outputs are obtained after the corresponding code evaluations. The resulting distribution of output responses was analyzed with the standard statistical analysis approach by assuming that the probability density function (PDF) of output is a normal distribution, which can be characterized by the expected value and standard deviation. Mathematically, the uncertainty in an individual output can be calculated through Eq. 2.4.

To verify this normality assumption, both graphical tools and quantitative analysis were used as the normality test approach for different output responses, including the core simulation results (e.g., effective multiplication factor k_{eff}, and power peaking factors). Graphical representations using histogram plot is provided to qualitatively visualize the

normality profile. Anderson-Darling goodness-of-fit test [22], which is a modification of the Kolmogorov-Smirnov test by assigning more weight to the tails of the distribution, is adopted to quantitatively analyse the deviation of the output responses from a perfect normal distribution. This method aims to calculate the A^2 value, which represents the distance from empirical cumulative distribution function (ECDF) to the cumulative distribution function (CDF) of a perfect normal distribution and has the following Eq. 2.12:

$$A^2 = -N - \frac{1}{N}\sum_{j=1}^{N}(2j-1)\left[ln\left(F(y_j)\right) + ln\left(1-F\left(y_{N-j+1}\right)\right)\right] \tag{2.12}$$

where N response data is arranged into the order of $y_1 \leq y_2 \leq y_3 \cdots \leq y_N$. $F(y_j)$ is the continuous cumulative distribution function from the corresponding perfect normal distribution. As previously mentioned, the perfect normal distribution is constructed using the same mean and standard deviation as the response distribution and thus $F(y_j)$ could be represented by Eq. 2.13:

$$F(y_j) = \frac{1}{\sqrt{2\pi}\sigma_y}\int_{-\inf}^{y_j} e^{-\frac{1}{2}\left(\frac{y-\bar{y}}{\sigma_y}\right)^2} dy \tag{2.13}$$

The hypothesis of normality is rejected if the computed A^2 value exceeds the critical threshold value [23].

For a given sample size, the confidence bounds of uncertainties on core output responses could be quantified using central limit theorem if normality assumption is valid. If a simple random sample size N is obtained from a normally distributed population with true mean μ and true standard deviation σ_{true}, then the following constructed parameter χ^2:

$$\chi^2 = \frac{(N-1)\sigma^2_{calc.}}{\sigma^2_{true}} \tag{2.14}$$

follows a chi-square distribution with N - 1 degree of freedom, where $\sigma^2_{calc.}$ is the sample variance. For a two-sided uncertain parameter, the criteria of 95% confidence level indicates that 95% of the χ^2 value is bounded inside the interval of $[\chi^2_{1-\alpha/2}, \chi^2_{\alpha/2}]$. The confidence

interval of the standard deviation σ_{true} could also be derived as Eq. 2.15:

$$\frac{(N-1)\sigma^2_{calc.}}{\sigma^2_{\alpha/2}} \leq \sigma^2_{true} \leq \frac{(N-1)\sigma^2_{calc.}}{\sigma^2_{1-\alpha/2}} \tag{2.15}$$

In this study, the relative uncertainties, namely the ratio of the standard deviation to the mean value, are calculated for some of the important physics parameters. By increasing the sample size, the confidence intervals can be narrowed down, as illustrated in Figure 2.3

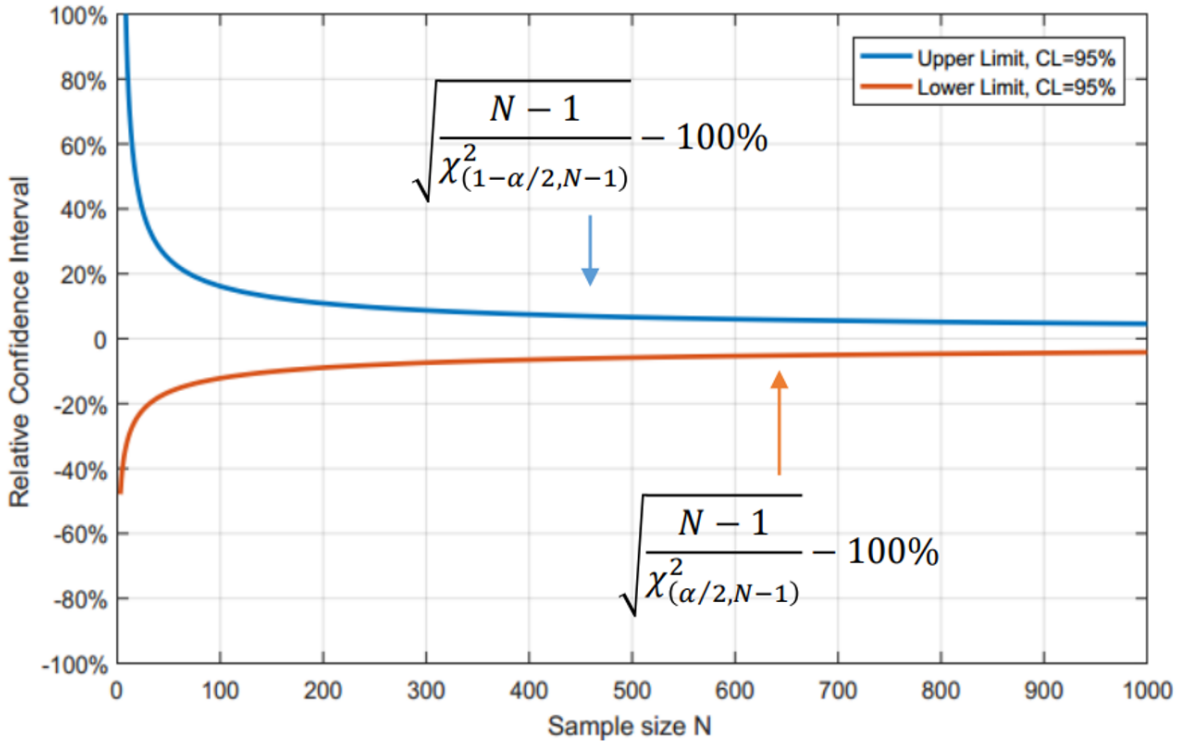

Figure 2.3 Confidence intervals corresponding to different sample size.

CHAPTER

3

INVESTIGATION OF CORRELATIONS BETWEEN DIFFERENT PHYSICS DOMAINS

Current LWR uncertainty quantification approaches do not consider multiphysics correlations. In the previous chapter we described the approach that will be studied for taking into account multiphysics correlations. This Chapter focuses on demonstrating the impact of various correlations between input parameters on PWR mini-core uncertainty analysis. The modelling of the PWR mini-core problem using conventional two-step core calculations is first presented. The global VCM for mini-core problem is constructed and the correlations between input parameters are evaluated. Finally, the impact of correlations on

core uncertainty quantifications are evaluated. Different correlations, including NK-FM, NK-TH, NK-FM-TH are considered and their impact on the estimation of uncertainties of core outputs are investigated.

3.1 Multi-physics Model of the PWR Mini-Core

The Organisation for Economic Co-operation and Development (OECD) Nuclear Energy Agency (NEA) has been developing an international benchmark of the light water reactor uncertainty analysis in modeling (LWR-UAM) to examine the uncertainty quantification and propagation methodologies with various simulation tools. The problem selected is a PWR mini-core problem based on the Three Mile Island unit 1 reactor. As shown in Figure 3.1, the PWR mini-core contains 9 fuel assemblies. Each assembly includes 208 fuel rods with a uranium enrichment of 4.12%, 16 guide tubes, and 1 instrumental tube in each assembly [17, 18].

The mini-core neutronic behavior is modelled using PARCS [24] and represented with 9 radial nodes based on one-node-per-assembly configuration. One ring of reflector assemblies is considered. Axially, the core is discretized into 24 equal axial nodes for the active core region plus 1 node each at the top and bottom of the core for the reflectors. The homogenized, burnup dependent cross-sections for fuel assembly and other few-group constants are generated with respect to different fuel temperature, moderator density, boron concentration, and the presence of control rod. The radial and axial reflectors are also modelled, while their corresponding few-group constants are assumed to be invariant as those generated at nominal state condition. The fluid dynamic and heat transfer calculations are performed using the TRACE code [25]. Each assembly is represented with a one-dimensional (1-D) PIPE, which models the average TH channel inside the assembly in TRACE code. The core is modelled using 9 parallel vertical PIPEs for the active core region and 1 PIPE for the radial reflector region. The inlet mass flow rate is assumed to be uniform

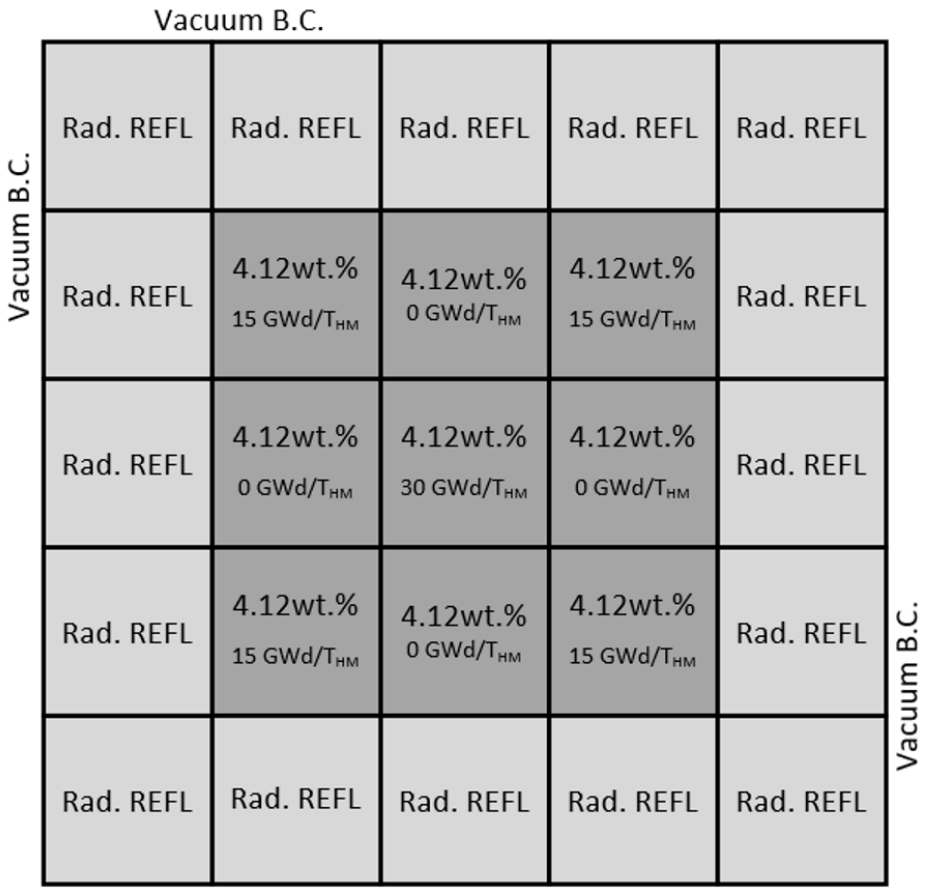

Figure 3.1 PWR mini-core radial layout.

and no cross-flow between different PIPEs are considered. The fuel assembly is represented by its average fuel rod. Generally, each of the fuel assemblies is modelled using its own heat structure component (FM). As shown in Figure 3.3, the discretization decision allows an exact one-to-one mapping among TH, FM, and neutronic nodes, which provides exact feedbacks without homogenization during multi-physics core simulation.

As shown in Figure 3.2, the standard industrial LWR core calculation scheme involves the calculations of assembly-level homogenized cross sections and other nodal parameters as first step and conducting whole core simulations using the homogenized data as the second step. The two-group assembly homogenized cross sections, and six delayed neutron groups were generated based on the ENDF/B-VII.1 using Polaris [26], a two-dimensional LWR lattice physics capability in the SCALE 6.2.1 code system [27]. The cross sections

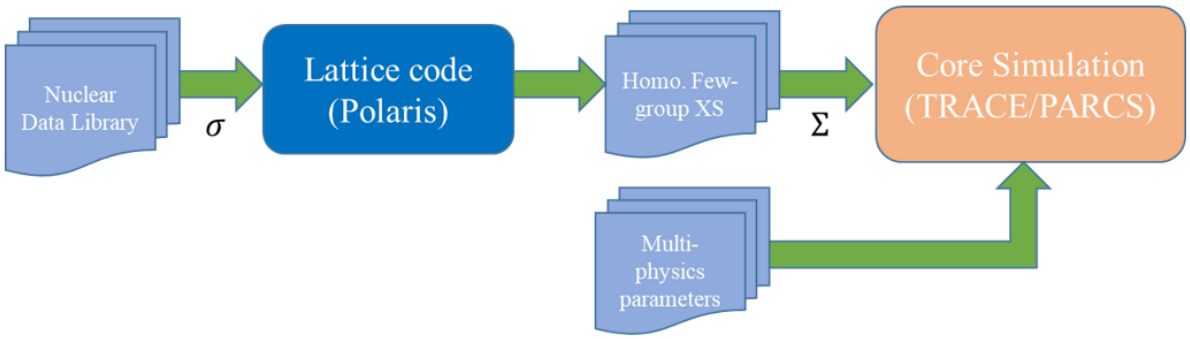

Figure 3.2 Conventional two-step LWR simulation approach.

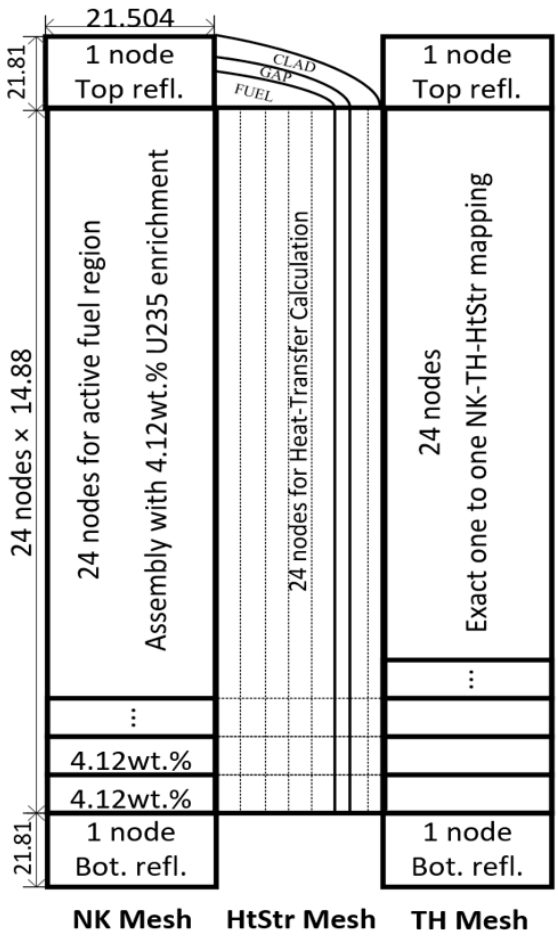

Figure 3.3 Heat conduction (HtStr) and thermal-hydraulics (TH) model, axial NK-FM-TH mapping.

(including transport, scattering, absorption, fission, xenon/samarium decay constants) were generated as a function of fuel temperature, moderator density, boron concentration,

and control rod insertion fuel assembly and reflectors. The ranges of those state variables are determined such that both steady state and transient conditions at both BOC and EOC are covered. Depletion calculation was performed with 15 burnup points ranging from 0 to 40 GWD/MTU. Due to the limitation in Polaris modelling capability, the spacer grid cannot be explicitly modelled. Therefore, an additional cladding has been placed surrounding the fuel rod to account for the effect of spacer grid based on spacer grid mass conservation.

An example of the parametric structure of the cross section of fuel assemblies is depicted in Figure 3.4. Let ρ be the moderator density, T_f the Doppler temperature, c the boron concentration, and Bu the burn-up, then the group homogenized macroscopic cross section in a specific state condition of (ρ, T_f, c, Bu) could be calculated with reference value Σ^r obtained at condition of $(\rho^r, T_f^r, c^r, Bu^r)$ and the derivatives with respect to different state variables as:

$$\Sigma(\rho, T_f, c, Bu) = \Sigma^r + \frac{\partial \Sigma}{\partial \rho}(\rho - \rho^r) + \frac{1}{2}\frac{\partial \Sigma^2}{\partial \rho^2}(\rho - \rho^r)^2 + \frac{\partial \Sigma}{\partial \sqrt{T_f}}(\sqrt{T_f} - \sqrt{T_f}^r) + \frac{\partial \Sigma}{\partial c}(c - c^r) + \frac{\partial \Sigma}{\partial Bu}(Bu - Bu^r) \tag{3.1}$$

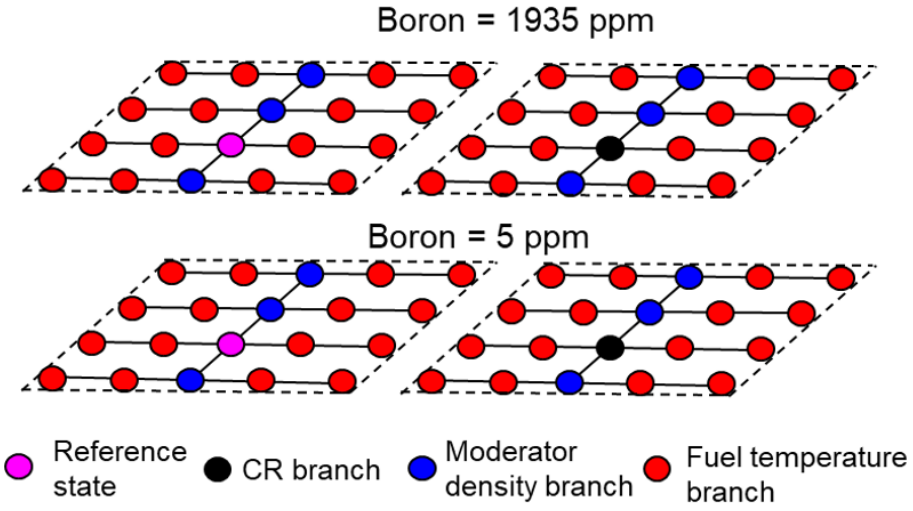

Figure 3.4 Cross section parameterization for fuel assemblies with control rod.

3.2 Events Description

Numerical simulation at steady state and control rod ejection under hot full power condition is studied in this paper based on the PWR mini-core model specification. At hot full power, the nominal power of the core at hot full power is 140.9 MWt with inlet mass flow rate of 915 kg/s under system pressure of 15 MPa. Critical boron concentration search is performed to bring the reactor core into a critical state, at which the control rod ejection transient is initiated. The control rod located in the central assembly is withdrawn at a constant speed for 10 seconds until it reaches a distance corresponding to 20% of the active core height. The total simulation time of the transient process is set to be 600 seconds such that the reactor core reaches another stable state.

3.3 Verification of VCM Generation

The first step of this study is to verify that the use of the VCM carries the correct correlation information and propagates input uncertainty through the two-step core simulation correctly. The following two cases are designed, and the uncertainty quantification results are compared to verify the effectiveness of the generated global VCM. Noted that at this step, only nuclear data uncertainty is considered, and the VCM only includes variables from the few-group constants.

- Case 1: n sets of few-group constants are generated using Polaris with uncertainty coming only from nuclear data uncertainty. The corresponding n core simulation runs are performed and the uncertainties of the output responses are calculated. Since this procedure involves the physical generation of the few-group constants, the uncertainties of output responses are used as references in the comparative analysis.

- Case 2: A global VCM is estimated using the few-group constants generated in Case 1, then another n sets of few-group constants are generated by re-sampling the

global VCM. The corresponding n core simulation runs are executed, and the output responses are analyzed and compared with results obtained in Case 1.

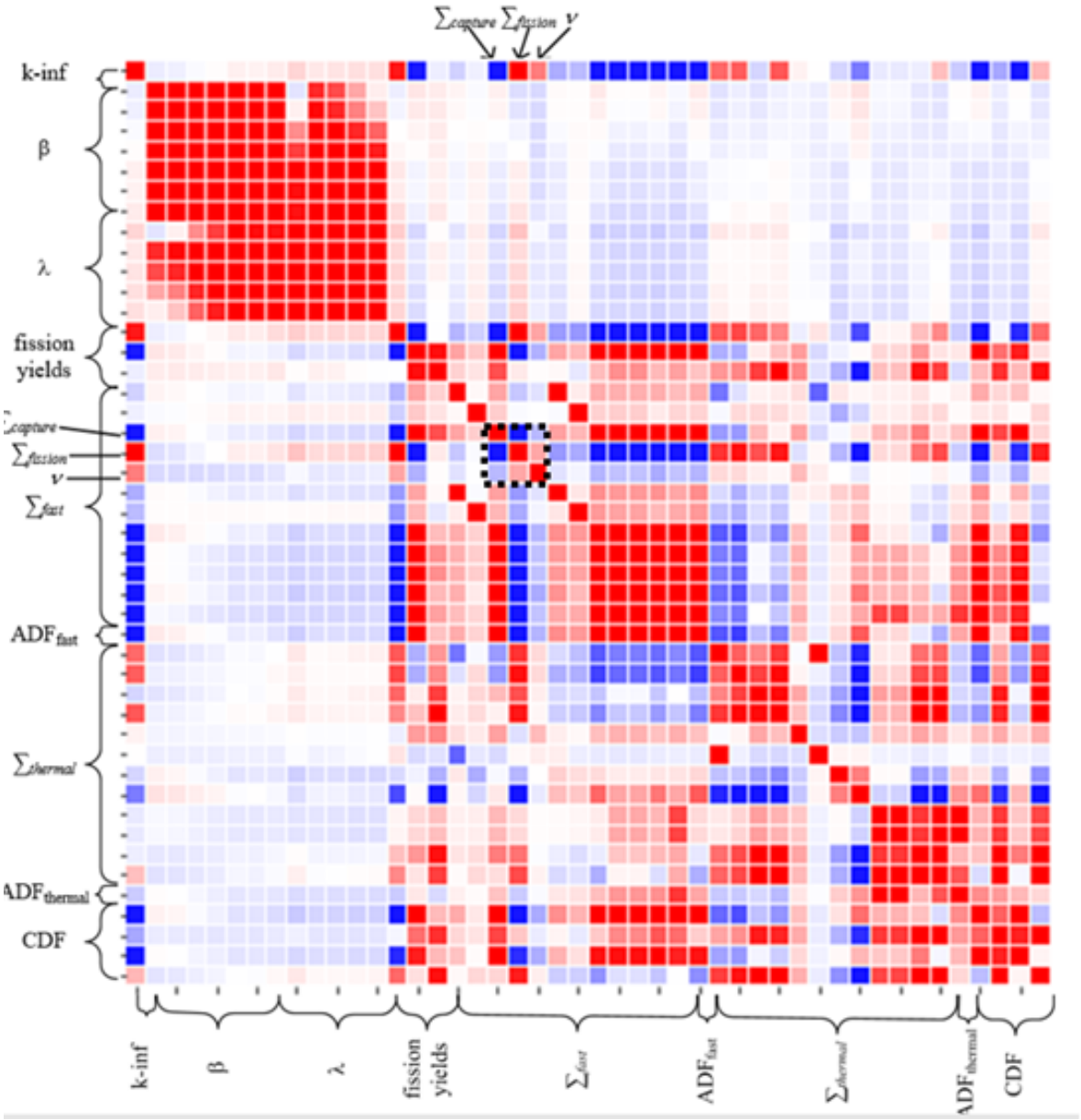

Figure 3.5 Correlation matrix of few-group constants.

It should be noted that such a correlation matrix is generated for all the data points of state variables, and the total number of such correlation matrices is 2×2×2×2×3=48, as

shown in Figure 3.6.

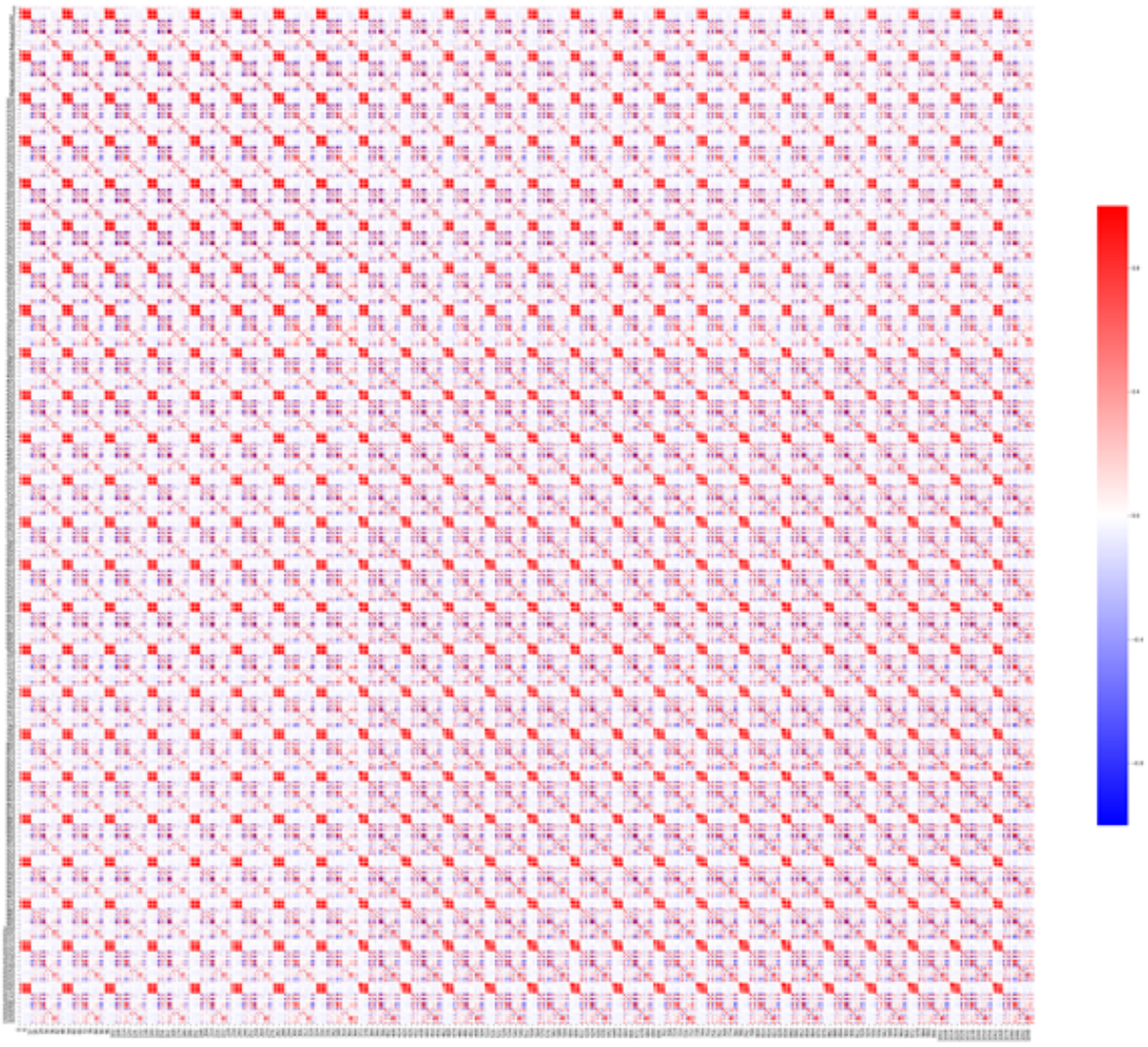

Figure 3.6 Correlation matrix for PWR mini-core problem.

It is worthwhile to mention that the few-group constants are functions of various state variables. The few-group constants at an arbitrary state are then calculated through interpolation using reference value and associated derivatives. Therefore, assembly few-group constants are generated using Polaris at various combinations of different values of the state variables, including two fuel temperatures, two moderator densities, two boron concentra-

tion, and two control rod states, at 3 burnup points (0, 15 and 30 MWD/T). Therefore, the generation of few-group constants in the lattice calculation is computationally expensive. In this study, $n = 500$ sets of few-group constants are generated. Figure 3.5 depicts the correlation matrix obtained at one state data point.

The correlation coefficient, ranged from -1 to +1, is a measurement of the strength of the associations between the two variables. A large absolute magnitude of the correlation coefficient means the variation of one variable has a strong impact on the variation of the other variable. Positive correlation indicates that both variables increase or decrease together, whereas negative correlation indictes an decrease of one variable will increase the other, and vice versa. It is observed that the 6 group delayed neutron fractions and decay constants are strongly correlated between them but are not strongly correlated with the rest of the few-group constants. Radiative capture cross-section has a negative correlation with assembly k_{inf}, while the correlations between k_{inf} and fission cross-section or the average total number of neutron release per fission are positive. The capture cross-section and fission cross-section are both components of the total absorption cross-sections, and as a result, a negative correlation coefficient is observed in Figure 3.5. In the lattice calculation, the fuel assembly is symmetric and a reflective boundary condition is used. As a result, the assembly discontinuity factors (ADFs) are the same for the four faces, and corner discontinuity factors (CDFs) with symmetrical locations and directions are also identical. Therefore, only two ADFs from different energy groups and 4 CDFs are input variables to be included in the global VCM.

Figure 3.7 shows the distribution of the diffusion coefficient extracted from the original few-group constants generated by Polaris. An inverse transform sampling of the cumulative density function of the standard normal variables is performed to obtained vectors of random samples, which is further multiplied by the lower triangular L matrix to obtain the vector of correlated input variables. The comparison of the KDE obtained from the original data and the re-sampling data is also presented in Figure 3.7, which shows that the

re-sampling data accurately recover the distribution of the original data.

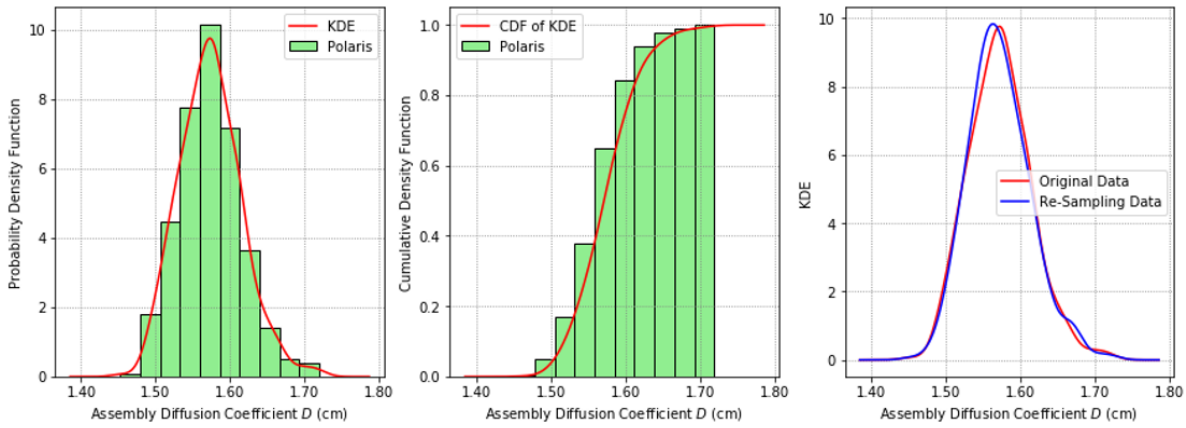

Figure 3.7 Distributions of original data (left), inverse transform sampling of CDF (mid.), and comparison of the distributions between original data and re-sampling data.

Both steady state simulation and control rod ejection transients are simulated under case 1 and case 2 configurations, where the original and re-sampling few-group constants are used, respectively. Figure 3.9 presents the comparison of the radial power distribution with associated relative standard deviations.

Figure 3.8 depicts the mean and associated uncertainties obtained with a different number of samples. It is found that the mean value and standard deviation converge after 100 samples, for both cases.

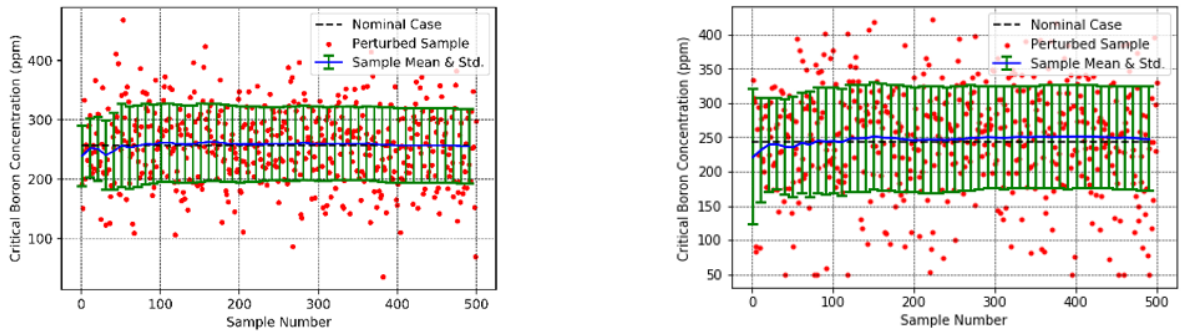

Figure 3.8 Running sample mean and uncertainty of the critical boron concentration at case 1 (left) and case 2 (right).

It can be observed that the mean value and uncertainty predicted with the few-group constants re-sampled using the global VCM agrees with those obtained using the original data quite well, despite that the re-sampling process tends to predict slightly larger uncertainty.

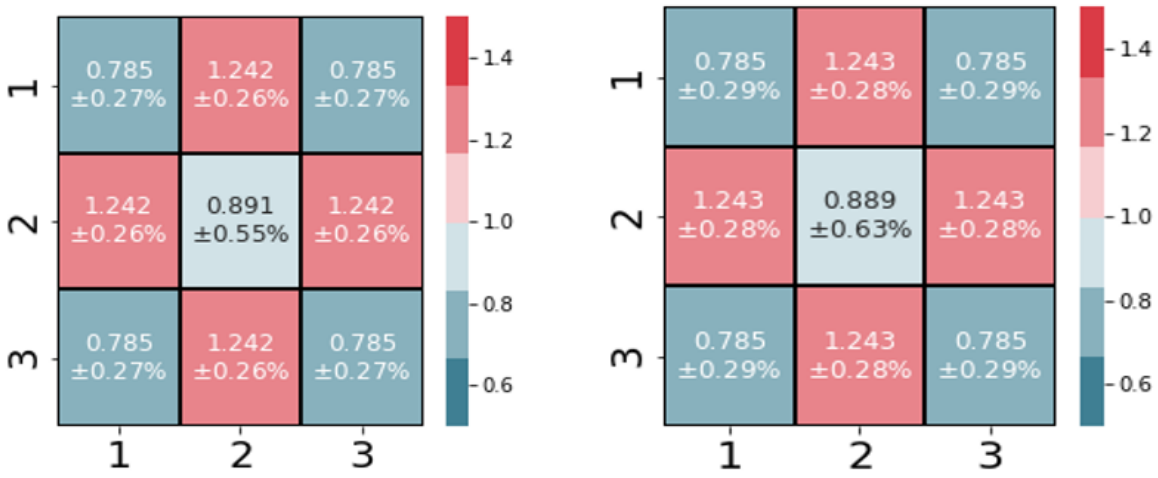

Figure 3.9 Radial power distributions with associated uncertainties corresponding to case 1 (left) and case 2 (right).

Figure 3.10 presents the time evolutions of peak reactivity, power and fuel centreline temperatures. It can be observed that for both cases, the mean values of the output responses agree perfectly with the nominal values. The trends of the time evolution of output responses agree with each other comparing the two cases. The 95% of the distribution of output responses are also plotted.

The mean values and associated uncertainties of the steady state critical boron concentration, power peaking factors, and the maximum values of transient reactivity, power, and fuel peaking centreline temperatures are calculated, as summarized in Table 3.1. The uncertainty of critical boron concentration is large at 63 pcm (25%) and 76 pcm (31%), respectively for case 1 and case 2. It can be found that the re-sampling the VCM tends to produce larger uncertainties on the output responses, while the source of this bias remains

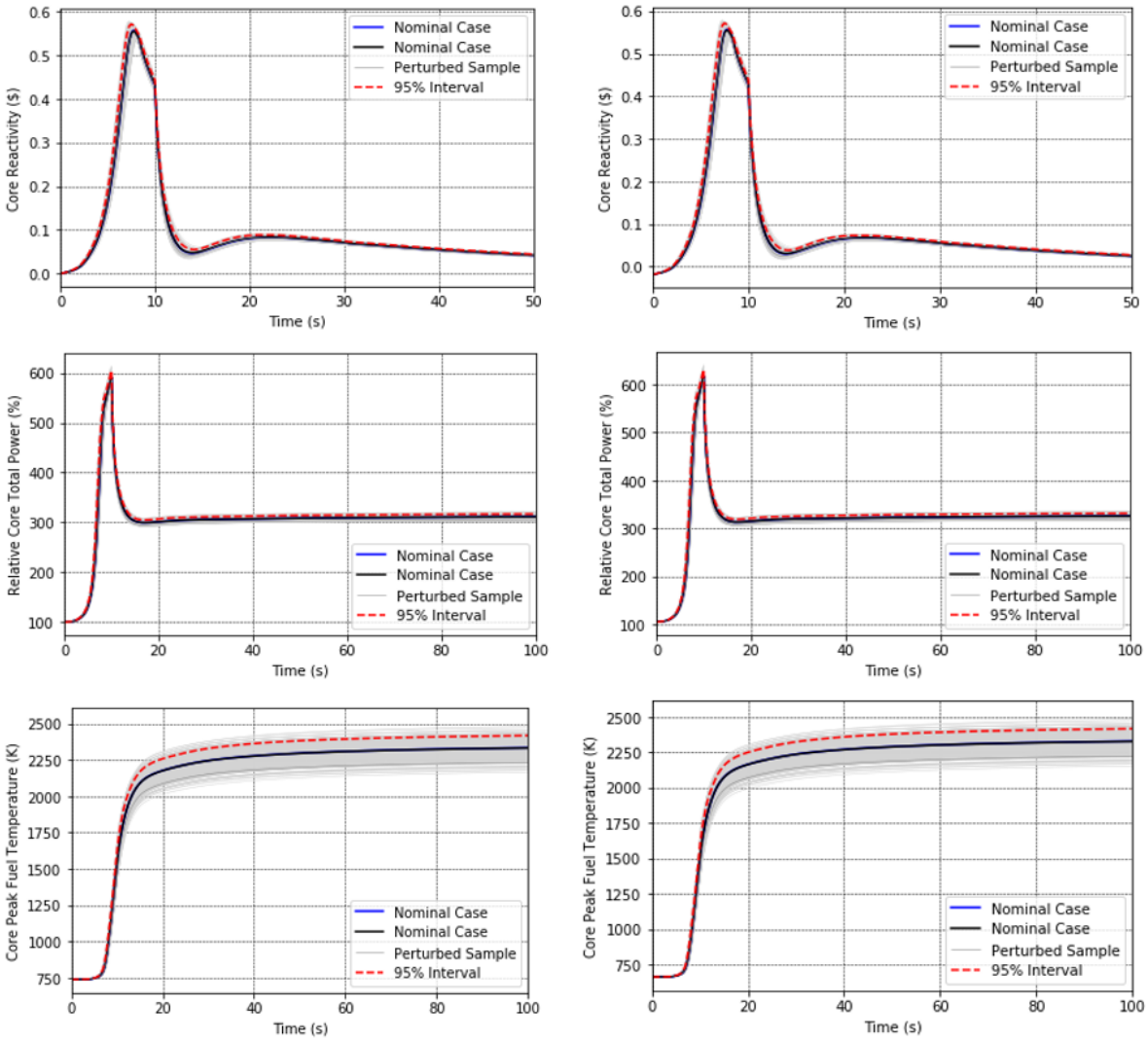

Figure 3.10 Time evolution of core reactivity, total core power, and peak fuel temperatures under case 1 (left) and case 2 (right) configurations.

unknown and requires more investigation.

3.4 Correlation of Input Parameters

Input parameters are correlated due to the fact that their uncertainties may stem from the same source. For demonstration purposes, the uncertainties of the fuel rod radius (R_{fuel}), the gap size (e) between fuel rod and cladding inner surface, and cladding thickness (T_{clad}) are considered and propagate to input parameters (X) from different physics domains. The

Table 3.1 Summary of core output responses comparing case 1 and case 2.

Output Responses	Case 1	Case 2
Steady state critical boron concentration	255±63 pcm	247±76 pcm
Steady state axial power peaking F_z	1.379±0.15%	1.385±0.19%
Steady state radial power peaking F_R	1.242±0.27%	1.243±0.28%
Transient peak reactivity	0.55794+0.02023 ($)	0.55863+0.02095 ($)
Transient peak power	5.91+0.206	6.18+0.209
Transient peak fuel temperature	2367+127.6 (K)	2364+135.9 (K)

few-group constants are generated from lattice physics code Polaris as described in Section 3.1. The manufacturing uncertainties related to geometry are given in Table 3.2.

Table 3.2 Summary of the geometrical manufacturing uncertainties considered for PWR mini-core problem.

Parameters	Distribution	Rel. Std.
R_{fuel}	Normal	0.99 %
T_{clad}	Normal	0.89%
e	Normal	5.25%

The thermal-hydraulic diameter (D_h), cross-sectional area (A_x) and wetted perimeter (P_w) of the TH channel, and the gap conductance (H_{gap}) are selected as representative TH and FM variables.

$$D_h = \frac{4A_x}{P_w} \tag{3.2}$$

$$P_w = 2\pi R_{clad} \tag{3.3}$$

$$A_x = P_{itch}^2 - \pi R_{clad}^2 \tag{3.4}$$

where, D_h is the thermal-hydraulics diameter, A_x is the cross-sectional area, P_w is the wetting perimeter of the TH channel, respectively. P_{itch} is the pitch of the fuel assembly and R_{clad} is the cladding outer radius.

$$H_{gap} = \frac{k_{gas}}{e} \tag{3.5}$$

$$e = R_{clad} - T_{clad} - R_{fuel} \tag{3.6}$$

H_{gap} can be simply modeled as the ratio of the gas conductivity k_{gas} to pellet-cladding gap width e. The gap width e can be further computed by R_{clad}, cladding thickness T_{clad} and fuel rod radius R_{fuel}. The input parameters for core multi-physics simulation, namely few-group neutronic constants, fuel modelling parameters and thermal-hydraulics parameters are computed. The corresponding global variance-covariance matrix is constructed. Latin Hypercube Sampling is performed to generate n=500 sets of samples and the corresponding core simulations are performed. Three different comparative studies are performed, with each study investigating the impact of correlations between different physics domains on core uncertainty quantification.

- Study 1: NK-TH correlations are considered. Uncertainties originating from geometrical manufacturing uncertainties are propagated into few-group constants and thermal-hydraulics parameters (D_h, A_x and P_w) to estimate the corresponding VCM. The VCM is re-sampled to propagate the uncertainty to steady state and rod ejection transient core simulations.

- Study 2: NK-FM correlations are considered with uncertainties originating from geometrical manufacturing uncertainties are propagated into NK few-group constants and FM parameters (H_{gap}) to estimate the corresponding VCM. The VCM is re-sampled to propagate the uncertainty to steady state and rod ejection transient

core simulations.

- Study 3: NK-TH-FM correlations are considered with uncertainties originating from geometrical manufacturing uncertainties.

3.4.1 NK-TH Correlation Study

The thermal-hydraulic model of the PWR generally requires the thermal-hydraulic diameter, cross-sectional area and volume of the TH channel as the inputs. In TRACE code, the PIPE channel represents ths average TH channel in the fuel assembly and the uncertainties of those three parameters are affected by the input uncertainties of fuel rod radius, gap thickness, and cladding thickness, as shown in Eq. 3.2 - 3.6. The global VCM can be constructed as shown in Figure 3.15. In order to quantify the impact of the correlations between NK and TH physics domains, the following two cases are designed:

- Correlated Case: The generated global VCM is sampled n times. The core simulations are performed with the sampled data and core output responses are analyzed.

- Uncorrelated Case: The uncorrelated NK-TH VCM is obtained by removing the covariance terms between NK and TH parameters, as shown in the right figure of Figure 3.15. The altered global VCM is then sampled for n times for realizations. Noted the generated realizations only reflect correlations in standalone NK or TH parameters, and the correlation between parameters of different physics domains has been removed. The corresponding core simulations are performed and output responses are analyzed. The sample size is 500 for both uncorrelated and correlated case.

Figure 3.12 and Figure 3.13 presents the steady state critical boron concentration, and radial power distributions at correlated and uncorrelated case, respectively. It can be found the standard deviation of critical boron concentration is about 20 pcm, which is small basically because only the fuel rod manufacturing uncertainties are perturbed.

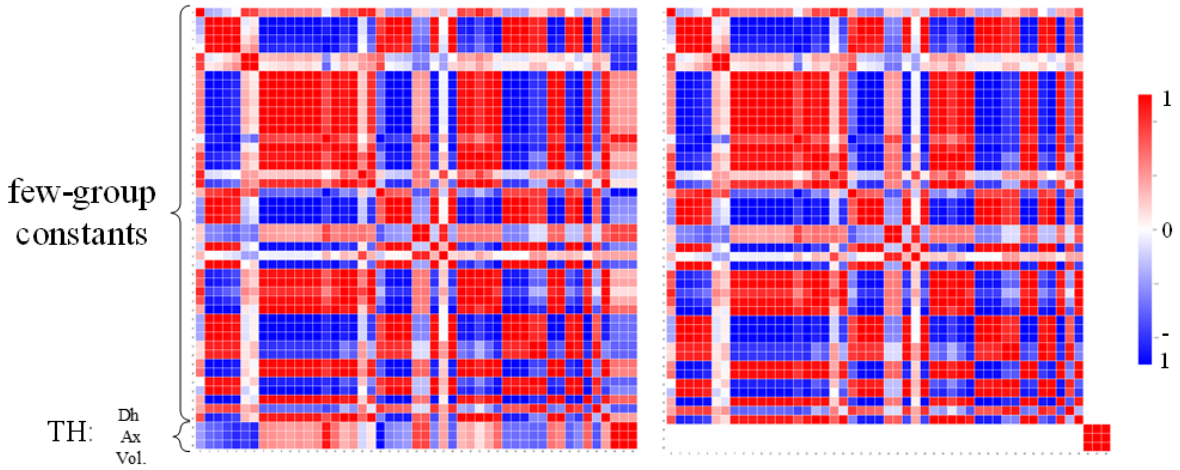

Figure 3.11 Time evolution of core reactivity, total core power, and peak fuel temperatures under case 1 (left) and case 2 (right) configurations.

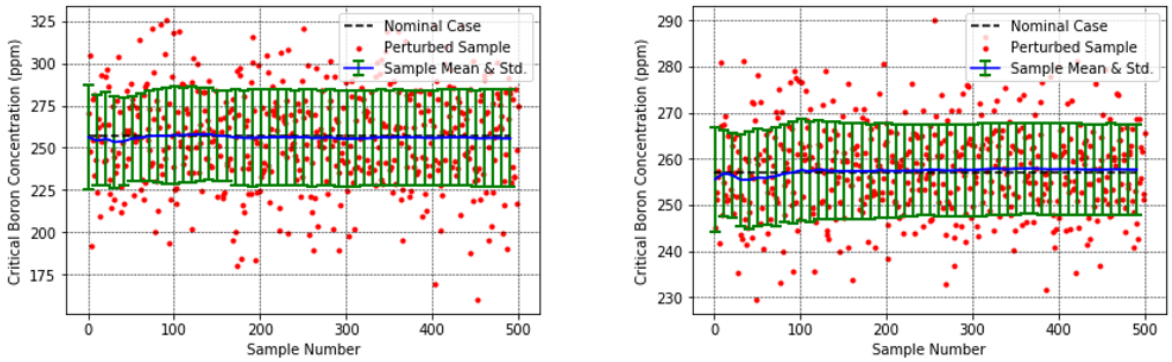

Figure 3.12 Running sample mean and uncertainty of the critical boron concentration at correlated case (left) and uncorrelated case (right).

Figure 3.14 shows the time evolution of peak fuel centerline temperatures. It is observed that the mean values are well-overlay with the nominal values. Table 3.3 summarizes the comparison of output responses obtained from correlated case and uncorrelated case. It is found that by implementing the correlation between different physics domains, the uncertainties of output responses are reduced compared to the case where the correlations are removed. Therefore, it can be concluded that by taking the correlations into account, more margins are obtained due to the reduction of output uncertainties.

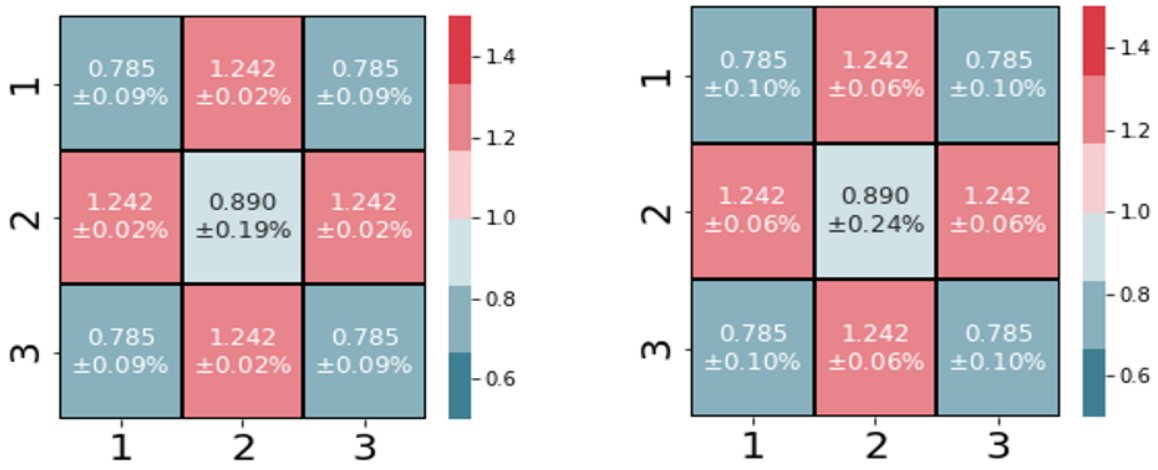

Figure 3.13 Radial power distributions with associated uncertainties corresponding at correlated case (left) and uncorrelated case (right).

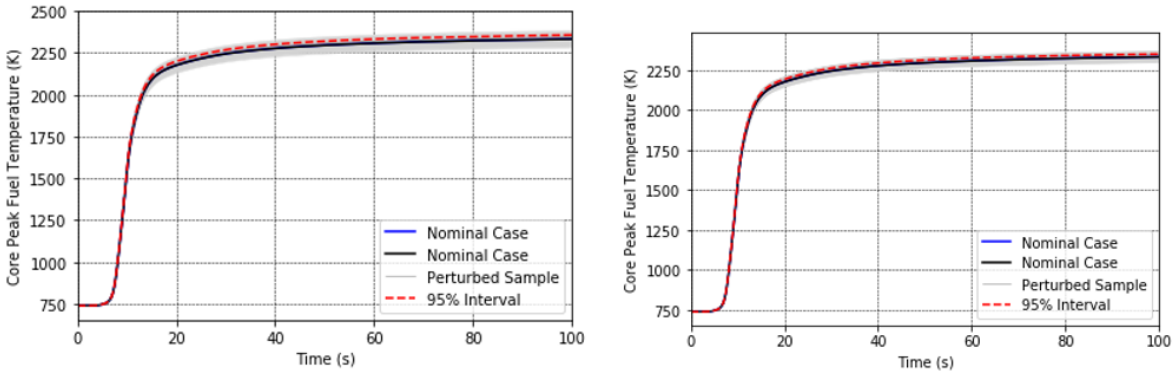

Figure 3.14 Time evolution of peak fuel temperatures under at correlated case (left) and uncorrelated case (right) configurations.

3.4.2 NK-FM Correlation Study

As described in Section 3.4, the gap conductance and few-group constants are correlated because their uncertainties originates from geometrical manufacturing uncertainties. Figure 3.15 presents the global VCM of the few group constant and gap conductance. It can be found that there are strong correlations between gap conductance and few-group constants, as have been depicted in Figure 3.15 . Especially, there exists a strong positive correlation between fission cross section and gap conductance (row 20, column 46).

Table 3.3 Impact of the correlated and uncorrelated input uncertainties on core outputs by taking into account NK-TH correlations.

Output Responses	Correlated case	Uncorrelated case
Steady state critical boron concentration	256±29 (pcm)	255±31 (pcm)
Steady state axial power peaking F_z	1.379±0.05%	1.379±0.05%
Steady state radial power peaking F_R	1.242±0.02%	1.242±0.07%
Transient peak reactivity	0.55736+0.00323 ($)	0.55734+0.00464 ($)
Transient peak power	5.91+0.08473	5.92+0.11102
Transient peak fuel temperature	2368+30 (K)	2376+41 (K)

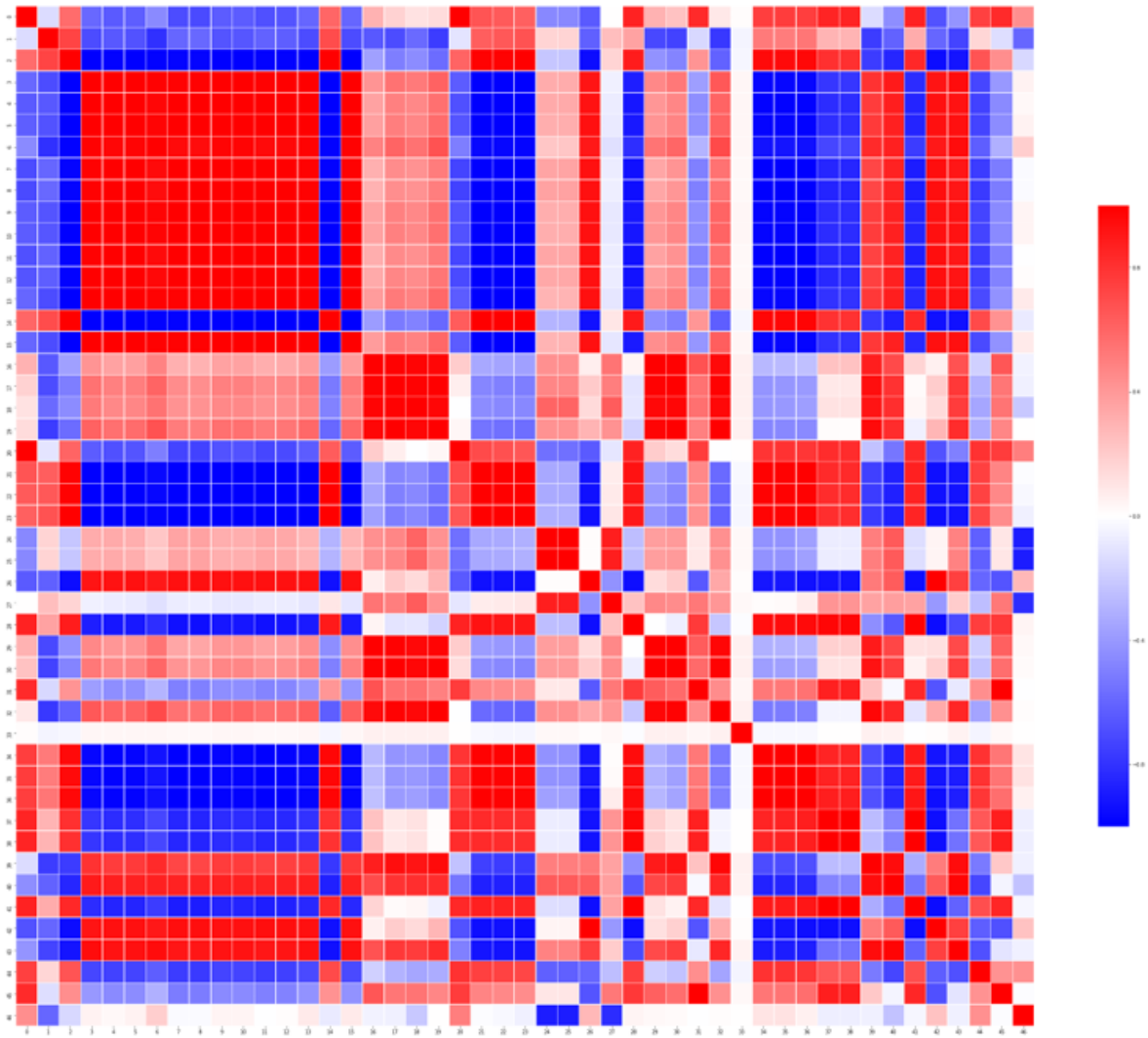

Figure 3.15 Correlation between few-group constants and gap conductance (NK-FM correlation).

Table 3.4 presents the impact of NK-FM correlation on core uncertainty analysis. It is observed that by taken into account the NK-FM correlations, the corresponding core responses is predicted with smaller uncertainties. For example, the uncertainty of peak fuel temperature is decreased by 9 K.

Table 3.4 Impact of the correlated and uncorrelated input uncertainties on core outputs by taken into account NK-FM correlations.

Output Responses	Correlated case	Uncorrelated case
Steady state critical boron concentration	260±35 (pcm)	256±36 (pcm)
Steady state axial power peaking F_z	1.387±0.06%	1.391±0.06%
Steady state radial power peaking F_R	1.245±0.08%	1.253±0.09%
Transient peak reactivity	0.55699+0.00353 ($)	0.55634+0.00465 ($)
Transient peak power	5.95+0.08994	5.96+0.11473
Transient peak fuel temperature	2390+33 (K)	2381+42 (K)

3.4.3 NK-FM-TH Correlation Study

In this study, the correlations between few group constants, gap conductance and thermal-hydraulics modelling input parameters (D_h, A_x, and P_w) are considered. The correlated case and uncorrelated case are designed and the uncertainties of PWR mini-core simulations are quantified, as summarized in Table 3.5. With the consideration of correlations, the core output responses are predicted with smaller uncertainties.

Table 3.5 Impact of the correlated and uncorrelated input uncertainties on core outputs by taken into account NK-TH correlations.

Output Responses	Correlated case	Uncorrelated case
Steady state critical boron concentration	259±40 pcm	250±48 pcm
Steady state axial power peaking F_z	1.371±0.20%	1.379±0.22%
Steady state radial power peaking F_R	1.232±0.30%	1.242±0.32%
Transient peak reactivity	0.55864+0.02304 ($)	0.55833+0.02415 ($)
Transient peak power	6.09+0.2175	6.15+0.2381
Transient peak fuel temperature	2367+56.8 (K)	2374+69.5 (K)

3.5 Summary

A consistent uncertainty propagation and quantification method for conventional two-step reactor core calculation approach is presented using the stochastic sampling method. A global VCM is developed to properly propagate the correlation between input parameters from different physics domains, whose uncertainties can be traced back into common sources. The correlation between NK, TH and FM parameters due to the manufacturing uncertainties in fuel rod fabrications are studied and propagated through core steady state and transient simulations. It can be observed that the correlations help to reduce the output uncertainties, creating more design margins.

CHAPTER

4

CONSISTENT UNCERTAINTY ANALYSIS OF THE TMI-1 REACTOR CORE

The consistent uncertainty propagation methodology has been applied in the PWR mini-core uncertainty quantification. The mini-core problem was selected as an demonstration because it is a simple reactor core, which only involves one type of fuel assembly and the core is formulated by only 9 fuel assemblies. This makes it possible to investigate the impact of NK-TH, NK-FM and NK-FM-TH correlations. In this Chapter, we apply the consistent uncertainty propagation methodology into a large scale PWR core to demonstrate that the proposed methodology is applicable to the uncertainty quantification of industrial nuclear power plants.

4.1 TMI-1 Reactor Core

The TMI-1 nuclear power plant is a PWR designed by Babcock & Wilcox with a rated power of 2772 MW_{th}. The power plant has a wet-recirculating system for cooling using two natural draft cooling towers. The reactor core consists of 177 fuel assemblies, and each fuel assembly has 208 fuel rods, 16 guide tubes, and 1 tube for the instrumentation. There are 11 types of fuel assemblies in the TMI-1 active core with various fuel enrichment (4.00%, 4.40%, 4.85%, 4.95%, and 5.00%) and configurations with regard to the configuration of the burnable poison (BP), gadolinia pins (GdO2+UO2) and control rod banks. The quarter core representation is depicted in Figure 4.1 where assembly H8 is located in the core center. Detailed geometry setup and fuel modelling parameters can be found in the benchmark specification [12].

4.2 Numerical Test Cases

Numerical test cases BOC and EOC steady state and control rod ejection under hot full power (HFP) condition were studied in this paper based on TMI-1 operational data for initial conditions. For steady-state calculations, boron concentration is set to be 1935 ppm and 5 ppm at BOC and EOC, respectively. At hot full power condition (HFP), control rod bank 1-6 (Figure 4.1) are completely withdrawn, bank 7 is completely inserted while the partial-length axial power shape rod (APSR) is 54% inserted. The rated power of the core at HFP is set to be 2772 MW with an inlet moderator temperature of 563 K. The mass flow rate is set to be 1.65 × 104 kg/s under a system pressure of 15 MPa, and coolant flowing into different TH channels are pre-calculated and used as fixed boundary conditions in this study [12].

The asymmetric rod ejection accident (REA) was studied to assess the safety performance of the TMI-1 core during a reactivity insertion transient. The transient is initiated by

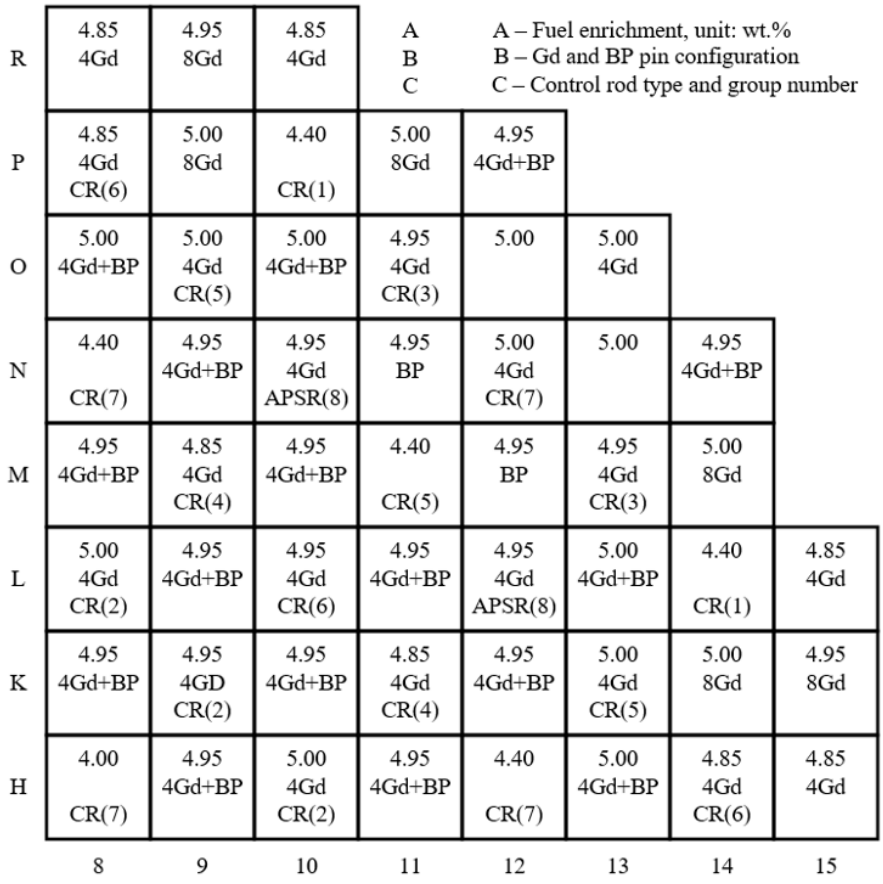

Figure 4.1 TMI-1 quarter core configuration.

a physical failure of a control rod drive mechanism housing such that the one of the highest worth control rod N12 is ejected by the reactor coolant system pressure. It is assumed that the transient starts at critical steady state, and the control rod is ejected from fully inserted position with a constant speed of 2380.8 cm/s to complete withdrawal position in approximately 145 ms, and results in a positive reactivity insertion that causes a power increase in the core. This transient simulation is vital from safety licensing point of view because if the reactivity insertion is large enough, the reactor may momentarily achieve prompt criticality, which may in turn lead to localized departure from nucleate boiling and fuel rod damage. Although the power increase will be limited by negative fuel temperature (Doppler) feedback, significant energy deposition in the fuel may occur during the event. In this study, the time evolutions of power, core reactivity, and peak fuel temperatures were

investigated to assess the core transient behavior.

The last case investigated in this study is the core cycle depletion calculation from BOC state to EOC state, as has been defined in the LWR-UAM Exercise 1 of Phase III. Reactor core is depleted at hot full power of 2771.9 MWth, with a nominal system pressure of 15.36 MPa. The mass flow rate through reactor core is assumed to be 16546.04 kg/s with inlet coolant temperature of 562.67 K. The estimated average fuel temperature and outlet coolant temperature is 921 K and 592.7 K, respectively. Control rod groups 1-6 are completed withdrawn, while group 7 and the axial power shape rod (APSR) is 90% and 30% withdrawn, respectively. The core is depleted for 664 EFPD with an estimated core average exposure of 42.06 GWD/MTU at EOC. The estimated critical boron concentration at EOC is 5 ppm.

4.3 Multi-Physics PWR Core Model

A reference TRACE/PARCS [28] model needs to be developed with a list of input uncertain parameters with associated distribution. This sub-section describes the specific neutronic-kinetic (NK) model, thermal-hydraulic (TH) model, as well as the coupling between the two. Generally, in order to perform a meaningful uncertainty propagation and quantification, the coupling scheme and reference model must be validated to be accurate enough. In the current stage, two coupling schemes were investigated, and the simulation results were compared in next Section to identify the impact of different coupling schemes on uncertainty quantification.

The TMI-1 core neutronic behaviour is modelled with PARCS. Radially, the core is divided into 21.81 cm × 21.81 cm nodes based on the one-node-per-assembly configuration plus the radial reflector. In total there are 181 nodes per axial plane. The core is discretised into 24 + 2 nodes axially: 24 equal-height computational nodes for the active core region and 2 nodes for the top and bottom reflectors. The 3-dimensional (3D) core burnup map has been provided in the UAM Phase III specification for the beginning of cycle (BOC) and

end of cycle (EOC) based on the reactor operational data. The average core exposure is 18 and 40 GWD/MTU at BOC and EOC, respectively.

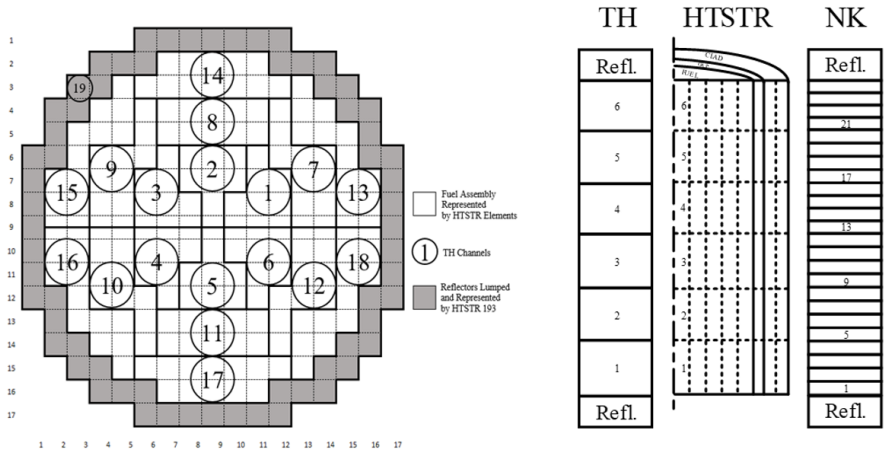

Figure 4.2 One Dimensional Channel model: TRACE TH, HTSTR models, and TH-HTSTR-NK mapping.

4.4 Uncertainty Analysis of PWR Steady State Simulation

Core k_{eff} and power peaking factors were selected as output responses of interest and results at nominal state were summarized in 4.1. It is worth mentioning that no boron concentration adjustment was performed for steady state calculations, and the k_{eff} at BOC is slightly higher than expected, partially because the core was modelled with only 18 TH channels, which tends to predict a smaller control rod worth compared to the detailed one TH channel to one fuel assembly model, as revealed by [29]. The core simulation at EOC was performed with equilibrium concentration calculation of Xenon and Samarium, which were efficient neutron absorbers and brought the core to be 1.71 % $\Delta\, k/k$ subcritical.

Input uncertainties considered in this study includes the geometrical manufacturing uncertainties and nuclear data uncertainty, as presented in A.1. Following the framework for consistent uncertainty propagation as proposed in Chapter 2, 100 samples are generated

Table 4.1 Core Physics Parameters at Nominal State.

	Nominal k_{eff}	Nominal F_Z	Nominal F_R	Nominal F_q
BOC	1.01501	1.01501	1.349	1.776
EOC	0.98290	1.190	1.402	1.674

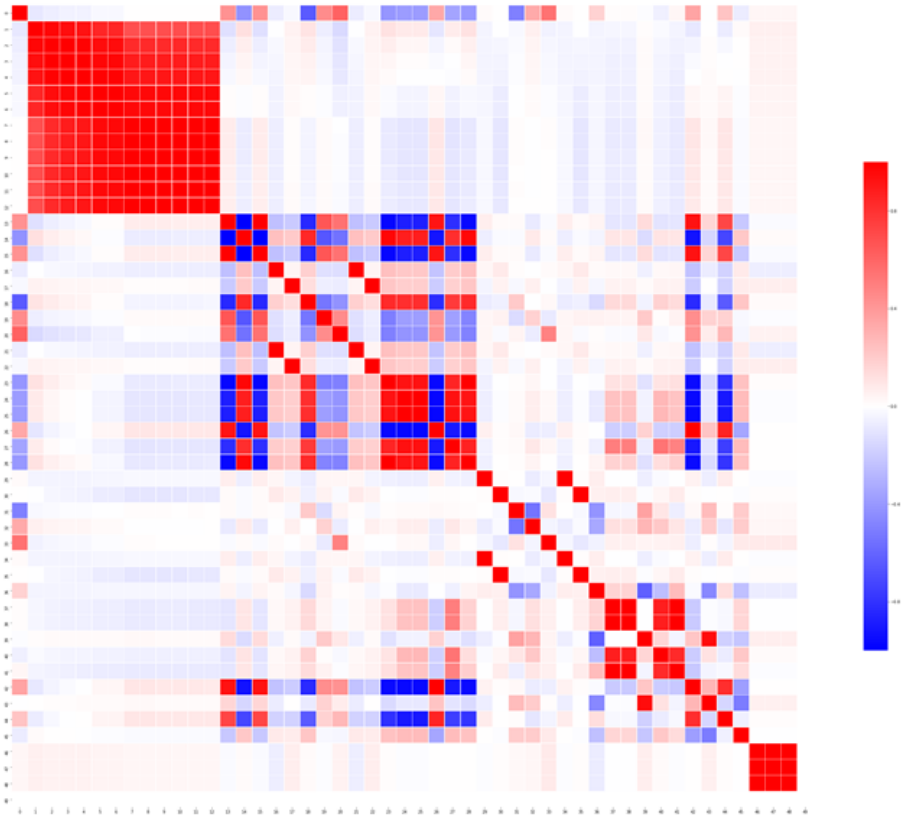

Figure 4.3 Correlation matrix of few-group constants, H_{gap}, D_h, A_x and P_w.

and passed into Polaris for lattice calculation. As a result, 100 sets of input parameters (few-group constants, H_{gap}, D_h, A_x and P_w) are obtained. The corresponding global VCM is computed as Eq. 2.3, as shown in Figure 4.3. By sampling the global VCM as described in Chapter 2 and 500 re-sampled input parameters are obtained, which are further passed into core multi-physics simulation using TRACE/PARCS as described in Chapter 4.3.

Figure 4.4 and 4.5 and shows the sample values with the mean and standard deviation of the core k_{eff}. The oscillation of the sample mean was reduced significantly after the initial

Table 4.2 Summary of the geometrical manufacturing uncertainties considered for TMI-1 large-scale core problem.

Parameters	Distribution	Rel. Std.
R_{fuel}	Normal	0.99 %
T_{clad}	Normal	0.89%
e	Normal	5.25%
Nuclear Data		ENDF/B-VII.1, SCALE 56-group VCM

400 samples and the standard deviation has also been stabilized. $N = 500$ burnup dependent sets of perturbed input parameters were generated for each of the assembly types. It should be noted that for the multi-physics thermal-hydraulics model, several fuel assemblies are represented with one TH channel. Therefore, the thermal-hydraulics parameters, namely the D_h, A_x, P_w, are computed for the average fuel rod of the TH channel. Uncertain fuel modelling parameters considered in this study were gap conductance with uncertainties from geometrical manufacturing uncertainties. The correlations between different physics domain are considered Following the Eq. 2.15, the true standard deviation σ_{true} of a two-sided distribution are bounded by [94% $\sigma_{calc.}$, 106% $\sigma_{calc.}$] with 95 % confidence level, where $\sigma_{calc.}$ is the standard deviation calculated from 500 samples. The uncertainty of σ_{true} could be reduced by increasing sample size (narrows down to [96% $\sigma_{calc.}$, 105 % $\sigma_{calc.}$] for sample size of 1000). It should be noted that the calculated confidence intervals are only valid given that the output response of interest is normally distributed.

Table 4.3 presents the overall results of core k_{eff}, axial power peaking factors (F_Z), and radial power peaking factors (F_R) for two core states given in the form of sample mean and relative standard deviation. A relatively small uncertainty (0.5 %) was found for most cases, while the uncertainties for F_Z at EOC and FR were relatively larger (>0.6 %), basically because the power peaking location changed among perturbed cases. For example, the axial peak power was observed at the 4th node from the bottom for 13% of the time, while

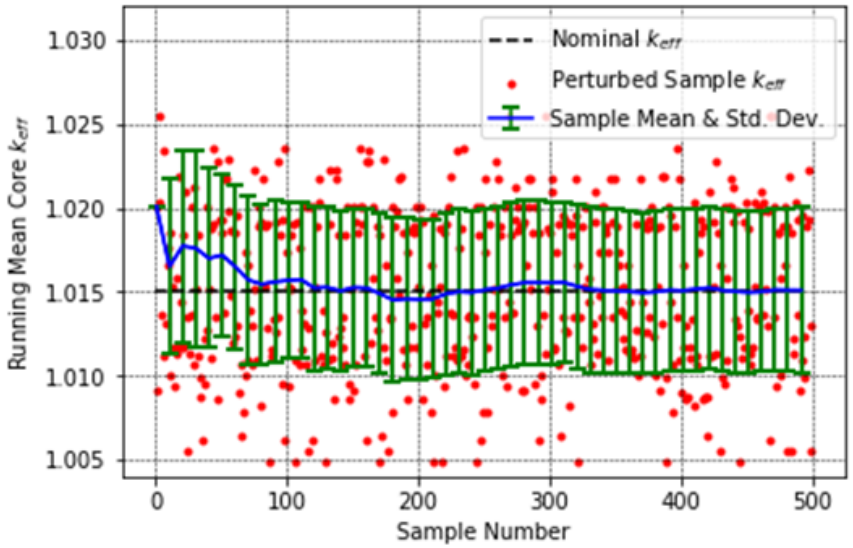

Figure 4.4 Running mean k_{eff} for HFP at BOC.

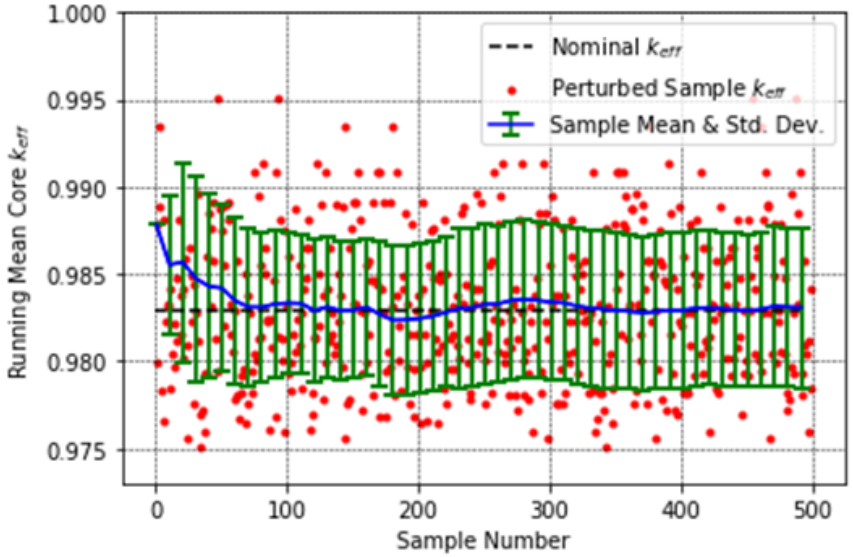

Figure 4.5 Running mean k_{eff} for HFP at EOC.

at the 5th for the rest.

Figure 4.6 shows the frequency histogram plot of core axial power peaking factor. The probability density function of those core responses were statistically estimated using kernel density estimation (KDE) and plotted in comparison with normal distributions, which are constructed with the calculated sample means and standard deviations. Anderson-Darling

Table 4.3 Summary of the geometrical manufacturing uncertainties considered for TMI-1 Reactor Core Steady State Simulation.

State	Statistics	k_{eff}	F_z	F_R
BOC	Mean ± rel. $\sigma_{calc.}$	1.01501±0.51%	1.32±0.52%	1.35±0.62%
	σ_{true}	[0.45%, 0.54%]	[0.49%, 0.55%]	[0.58%, 0.66%]
	AD normality test		Pass	Pass
EOC	Mean ± rel. $\sigma_{calc.}$	0.98295±0.45%	1.19±0.63%	1.40±0.82%
	σ_{true}	[0.42%, 0.48%]	[0.59%, 0.67%]	[0.77%, 0.87%]
	AD normality test	Pass	Pass	Pass

normality tests are also performed for the keff and power peaking factors. The calculated A2 for core responses are less than 0.757, as shown in Table 4.3. It could be interpreted as that the distance from ECDF of the sample distribution to the CDF of the re-constructed perfect normal distribution is less than the critical threshold (0.757) and the probability of observing an equal or even smaller distance is greater than the pre-determined significant level of 0.05. It could be concluded that the sample populations of all the four core responses are significantly drawn from normal distributions, which could be fully described by providing the means and standard deviations.

It should be noted that the peaking location in both radial and axial power distribution may be varied sample by sample, and there are two approaches in reporting the power peaking factors as shown in Table 4.4. In the first method, as denoted as M1, the peaking factor distribution was constructed from maximum relative power taken from the core results regardless the peaking location. In the second method (M2), the peak location was identified first based on the mean power distribution over all samples, followed by the peaking factor selected and used to form the distribution. It was found that the distribution constructed with method M2 were always closer to the perfect normal distribution by having smaller A2 and larger p-values, which is expected because different nodal locations

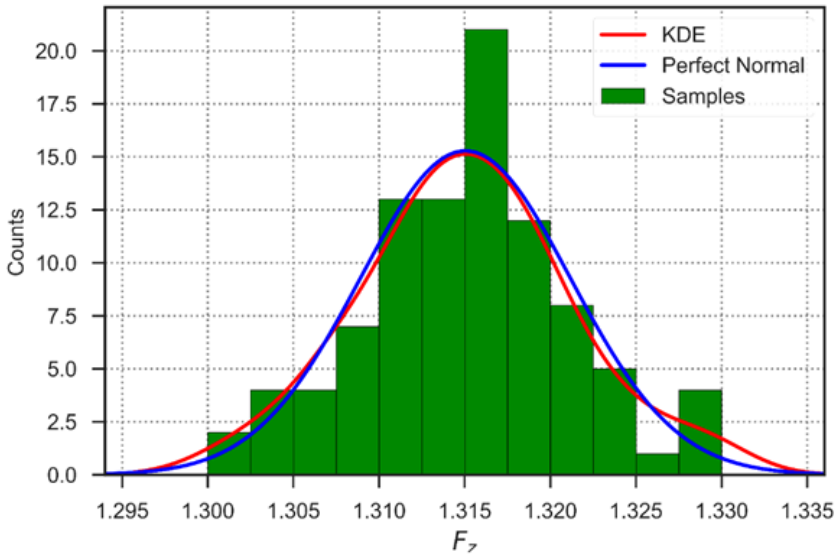

Figure 4.6 Frequency histogram of core key axial power peaking factors at HFP EOC state.

corresponds to different assembly compositions and material properties.

Table 4.4 A^2 and corresponding $p-values$ for power peaking factors at various core states.

State	F_z (M1)	F_z (M2)	F_R (M1)	F_R (M2)
BOC A^2	0.251	0.265	0.236	0.322
EOC A^2	0.365	0.463	0.536	0.368
BOC $p-values$	0.212	0.439	0.155	0.356
EOC $p-values$	0.433	0.531	0.326	0.461

Planar integrated axial power profiles under both states are presented in . At BOC, the fuel in the middle of the core was burnt at a higher rate, which leaded to the reduction of axial power peaking factor over the cycle and flattened the axial power profile at EOC. Higher relative uncertainties of axial nodal power at the bottom and top of the core were observed compared to those obtained in core axial center, which is due to the fact that the mean power in those regions were lower and the power gradients are larger.

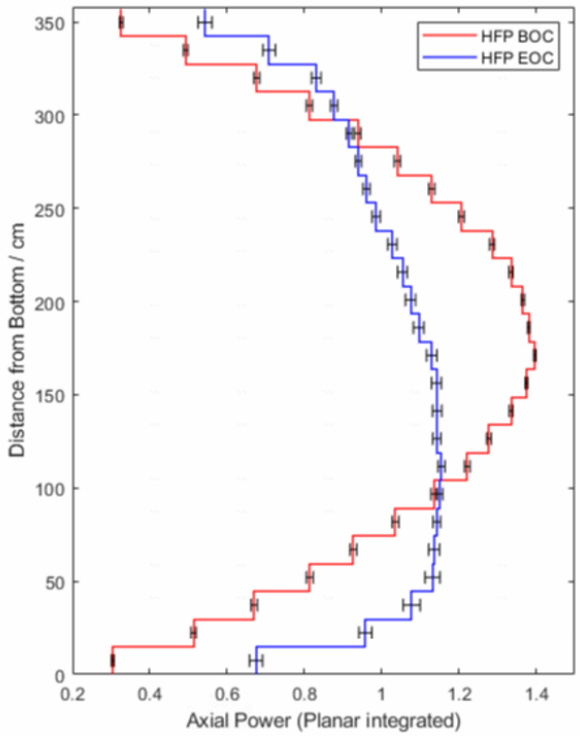

Figure 4.7 Core axial power under HFP BOC and HFP EOC steady states.

The assembly-wise power map in the radial direction, including the mean and associated uncertainty, is given in Figure 4.8 and 4.9. Although the core assembly configuration is 1/8th symmetrical configuration, the radial power map is 1/4th symmetrical. This is basically because different assemblies are lumped into one TH channels and the core TH configuration is quarter symmetrical. The maximum radial assembly power was found to be in the same location of L11 in both BOC and EOC conditions, because assembly L11 is far away from the core periphery and control rods surrounding L11 are completely withdrawn or partially inserted axial power shape rod. The lowest power was found at the central assembly in all cases because control rod bank 7 was fully inserted, as a result, relative uncertainty of assembly power was found to be comparatively large in centre of the core. Generally, uncertainties tended to be more significant at locations where large radial power gradients were observed, for both BOC and EOC. The fuel composition and enrichment also have a pronounced impact on the evaluation of uncertainty. For example,

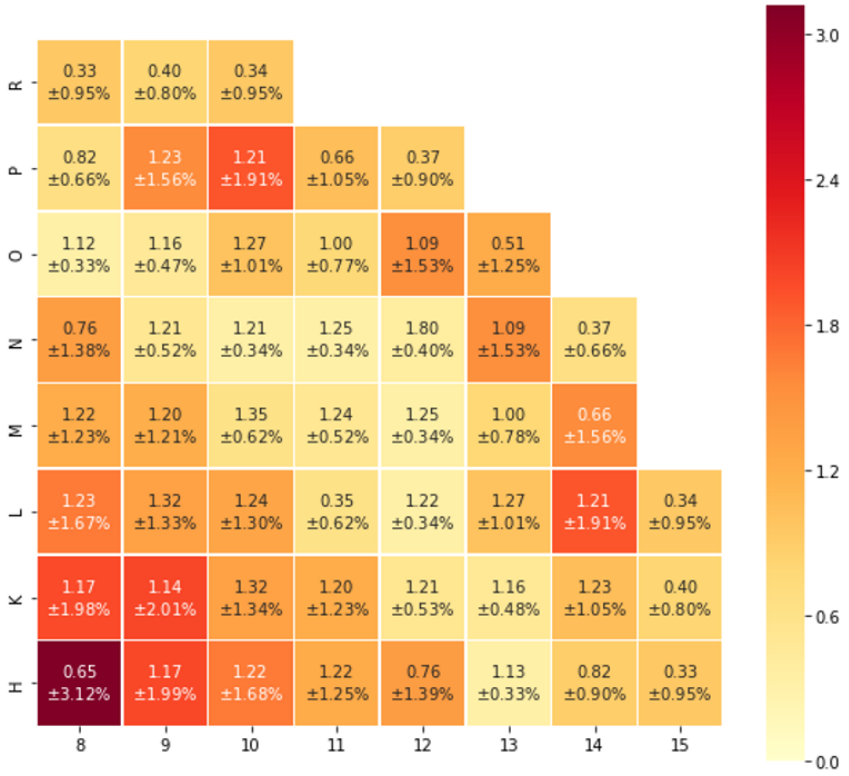

Figure 4.8 Radial power distribution at BOC .

larger uncertainty was observed at BOC compared to EOC, as fuel assemblies are higher enriched at BOC condition.

The impact of correlations between different physics domains are quantified. Table 4.5 summarizes the results of core key parameters with associated uncertainties calculated with and without consideration of NK-FM-TH correlations. It is observed that the core output responses are predicted with larger uncertainties when the correlations are ignored. The uncertainties of core outputs due to few-group constant only are also quantified, which are found to be close to the result observed when uncertainties from all three physics domains are considered. The contributions of uncertainty from nuclear data and fuel modeling parameters were also quantified. Table 4.5 also summarizes the results of core responses with associated uncertainties calculated when only nuclear data or a single fuel modeling parameter were treated as the uncertain variable. As expected, NK few-group constants

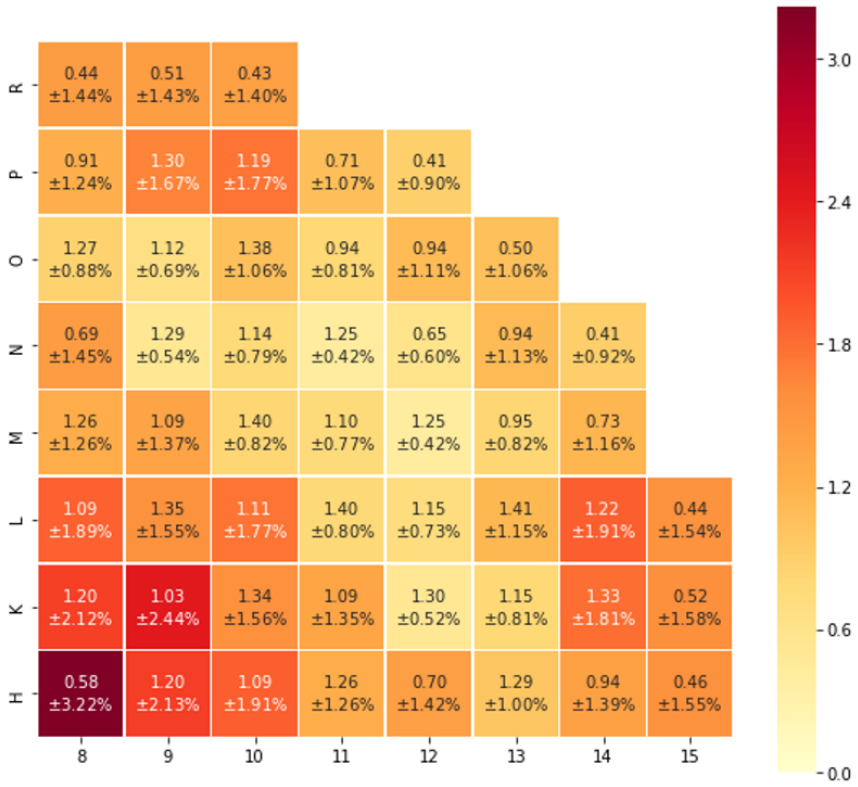

Figure 4.9 Radial power distribution at EOC.

have the largest contribution to all three core output responses. FM (H_{gap}) and TH related parameters have only small impact (<0.11%) on core steady state k_{eff} and power peaking factors.

4.5 Uncertainty Analysis of PWR Transient Simulation

For the REA analysis, the uncertainties of both nuclear data and fuel modeling parameters were propagated through transient safety calculation using the TRACE/PARCS multi-physics model and the uncertainty quantification was performed for three quantities of interest, including the net core reactivity, core power and peak fuel temperature. A sufficiently long simulation time of 70 s was selected to ensure it covers maximum value of the peak fuel temperature, as the net reactivity and normalized core power reach the asymptotic

Table 4.5 Summary of uncertainty quantification on selected core parameters at steady state simulations (numbers given in mean ± relative standard deviation).

Source of uncertainty	State	Sample k_{eff}	Sample F_Z	Sample F_R
Correlated	BOC	1.01501±0.51%	1.32±0.52%	1.35±0.62%
	EOC	0.98295±0.45%	1.19±0.63%	1.40±0.82%
Uncorrelated	BOC	1.01511±0.53%	1.32±0.52%	1.35±0.64%
	EOC	0.98290±0.46%	1.19±0.64%	1.40±0.86%
NK few-group constants only	BOC	1.01503±0.50%	1.32±0.50%	1.34±0.53%
	EOC	0.98294±0.43%	1.19±0.53%	1.41±0.51%
FM only	BOC	1.01511±0.03%	1.31±0.11%	1.35±0.09%
	EOC	0.98284±0.01%	1.19±0.09%	1.40±0.08%
TH only	BOC	1.01496±0.03%	1.32±0.06%	1.35±0.02%
	EOC	0.98290±0.04%	1.19±0.05%	1.40±0.03%

value at a significantly faster rate within 5 seconds. According to the Wilk's formula, $N = 93$ perturbed cases were generated by sampling the global VCM as generated in using the LHS approach, each associated with one set of perturbed cross sections produced in the lattice calculation. The simulation results of the nominal cases, where no uncertainties were taken into consideration, are plotted in the black line in through Figure 4.10 to Figure 4.15. It was found that the net core reactivity peaks at approximately 145 ms into the transient with the maximum values of 0.40 $ and 0.41 $ at BOC and EOC, respectively, as seen in Figure 4.10 and Figure 4.11. As seen in Figure 4.12 and Figure 4.13, the peak core power at EOC is 38 % higher than the nominal value, which exhibits a more dramatic increase than that at BOC (29 % higher than the initial power) due to the larger reactivity insertion. Figure 4.14 and Figure 4.15, respectively, show the peak fuel temperature during the REA transient at BOC and EOC. Both curves reach the asymptotic value after 50 s into the transient and the peak value at BOC is 2606.1 K, which is 800 K higher than that at EOC because of the high

reactivity insertion and smaller gap conductance at BOC. It is worth mentioning that in this study the peak fuel temperature is defined as the maximum temperature of fuel that can be found in any location of the core and thus is a location-free value. Consequently, when the peak location of the fuel temperature changes during the transient, it can cause "discontinuity" in the time evolution curve of the fuel temperature. For example, the "jump" that occurred at 5-10 s for almost all cases at EOC is caused by the shift of the fuel temperature peak location from L11 to M12.

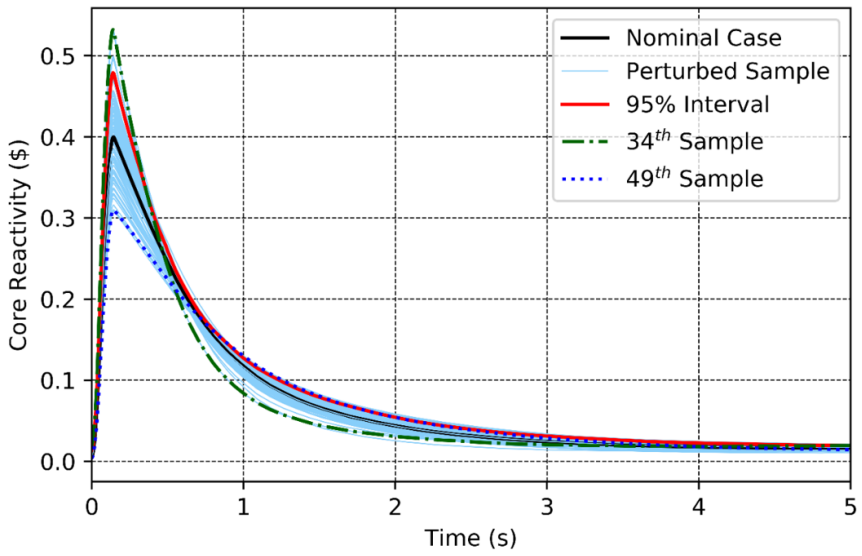

Figure 4.10 Core net reactivity during transient, initiated from HFP at BOC.

At the BOC, the predicted peak fuel temperature observed in the best estimated calculation is 2598 K with additional 106 K of 95 % confidence, as summarized in Table 4.6. A similar comparative analysis is performed to investigate the impact of NK-FM-TH correlations on core uncertainties quantifications. As presented in Table 4.6, the prediction of 95 % confidence interval of peak fuel temperature is 2704 and 2741 at BOC, respectively for the cases when correlations are considered and removed. Consistent conclusion as previous PWR mini-core cases can be drawn, which indicates that the uncertainties and 95 % safety limits of core outputs tends to be smaller when correlations are considered. By separately

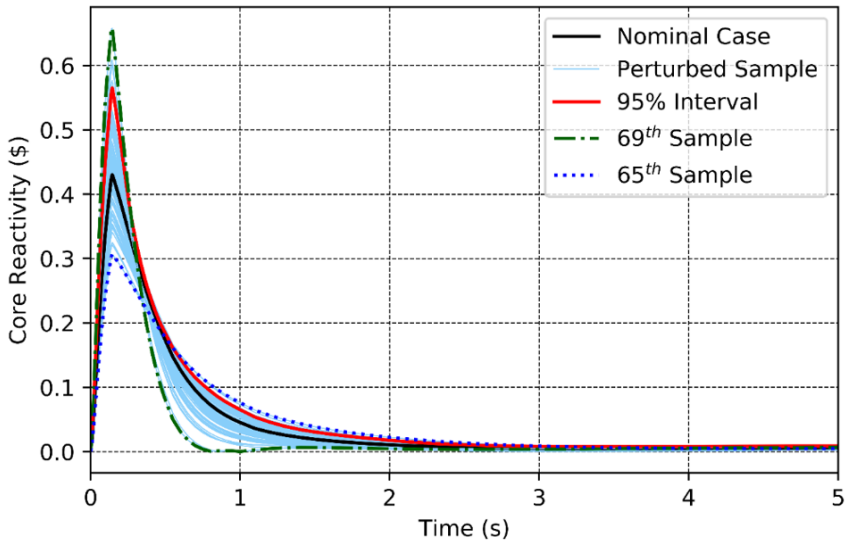

Figure 4.11 Core net reactivity during transient, initiated from HFP at EOC.

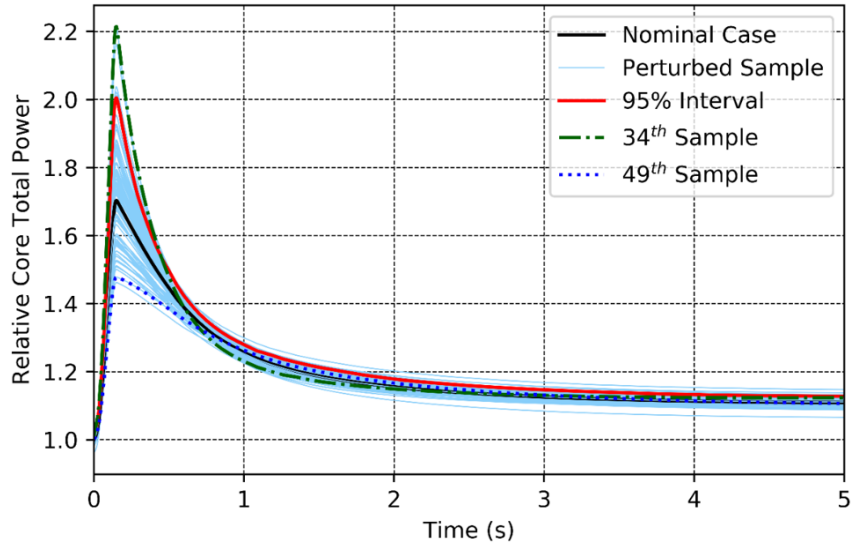

Figure 4.12 Normalized core power during transient, initiated from critical HFP at BOC.

perturbing the input parameters from different physics domains, the contribution to core output uncertainties due to different input parameters can be evaluated, as shown in Table 4.6. It is observed that the uncertainties of peak core reactivity and peak power during the transient is mostly contributed by NK few-group constants. The uncertainty of peak fuel temperature is also mostly contributed by NK few-group constants, but FM (H_{gap}) and

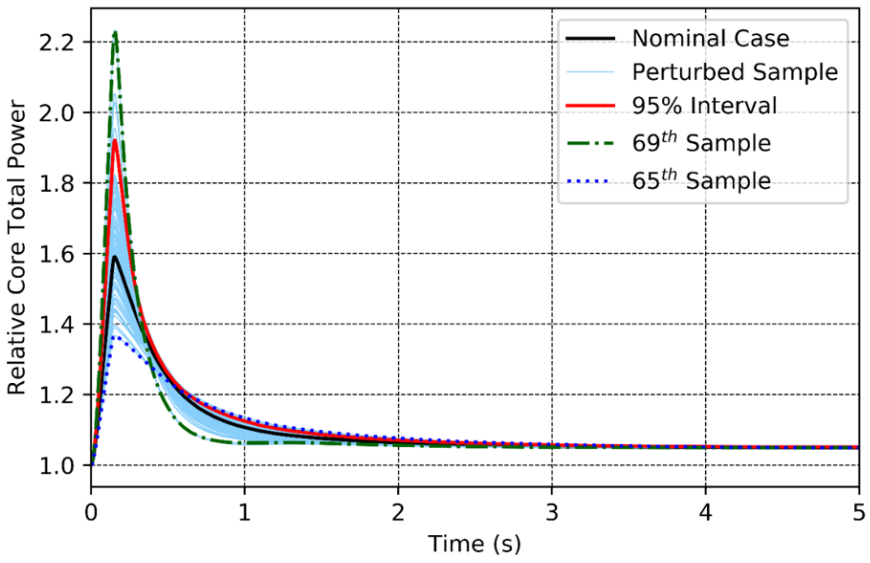

Figure 4.13 Normalized core power during transient, initiated from critical HFP at EOC.

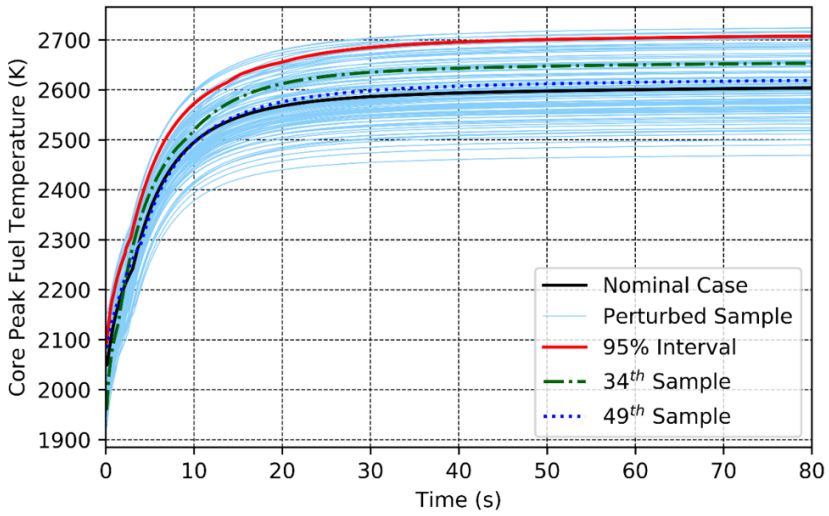

Figure 4.14 Peak fuel temperature during transient, initiated from HFP at BOC.

TH (h_d, P_w and Vol) related parameters also have non-negligible contributions. It is also observed that H_{gap} shows larger impact on peak fuel temperature at BOC than EOC, which is reasonable due to larger gap size at BOC.

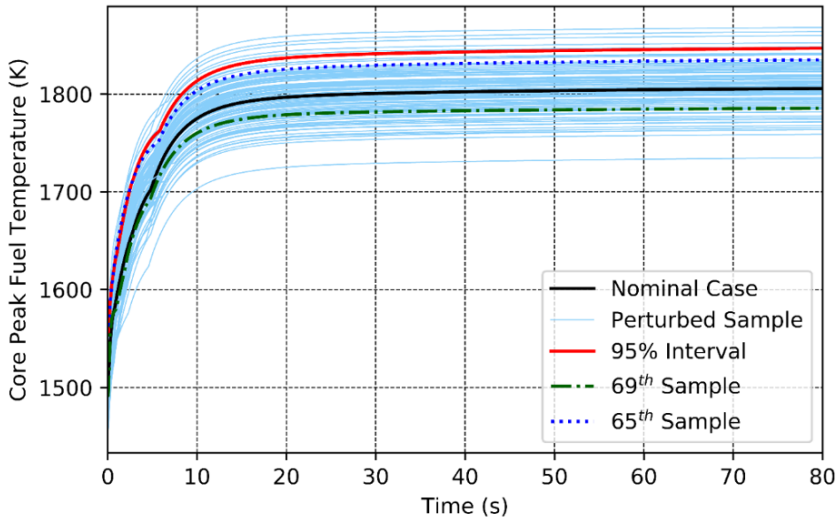

Figure 4.15 Peak fuel temperature during transient, initiated from HFP at EOC.

Table 4.6 Summary of uncertainty quantification for TMI-1 REA transient simulations (numbers given in mean + [95th/95% tolerance limit - mean]).

State	Peak Core Reactivity ($)	Peak Core Total Power	Peak Fuel Temperature (K)
Correlated BOC	0.405421+0.07253	1.71+16.3%	2598+106
Correlated EOC	0.418030+0.10068	1.65+24.3%	1810+89
Uncorrelated BOC	0.405389+0.07356	1.69+17.1%	2593+148
Uncorrelated EOC	0. 418145+0.10165	1.63+25.5%	1815+95
NK only BOC	0.405411+0.06132	1.70+14.3%	2590+89
NK only EOC	0.418102+0.10056	1.64+20.3%	1813+73
FM only BOC	0.405416+0.00153	1.70+0.41%	2593+40
FM only EOC	0.418032+0.00568	1.64+1.23%	1812+26
TH only BOC	0.405403+0.00093	1.71+0.23%	2594+11
TH only EOC	0.418001+0.00165	1.64+0.30%	1813+13

4.6 Uncertainty Analysis of PWR Cycle Depletion Simulation

Figure 4.16 presents the core burnup distribution predicted by PARCS/PATHS [30] in the unperturbed case. The reference solutions of assembly burnups can be found in LWR-UAM benchmark specification, and the maximum relative error of the simulation results is found to be -1.39%. The calculated critical boron concentration at EOC is 38 ppm, which compares favorably with the reference solution with an error of 33 ppm.

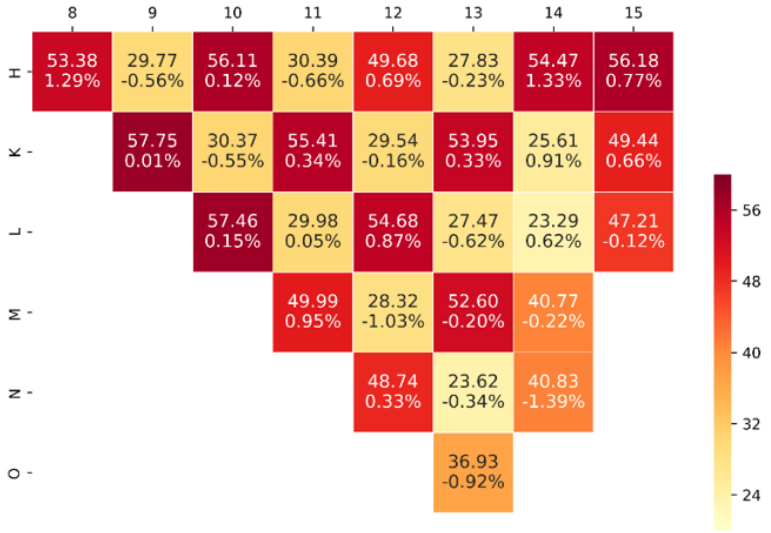

Figure 4.16 Core Burnup Distribution and Relative Error at EOC.

The burnups at different assemblies are calculated with associated uncertainties, as shown in Figure 4.17. It is found that most of the assembly burnups pass Anderson-Darling normality test. The maximum uncertainty of assembly burnup is found to be 2.87%, which is 0.83 GWD/MTU in equivalence and is obtained from assembly L13. Figure 4.18 shows the assembly bunrups with associated uncertainties when NK-FM-TH correlations are ignored. In general, the NK-FM-TH correlations has negligible impact on the prediction of mean assembly burnups at EOC during cycle depletion and tends to reduce the associated

uncertainties.

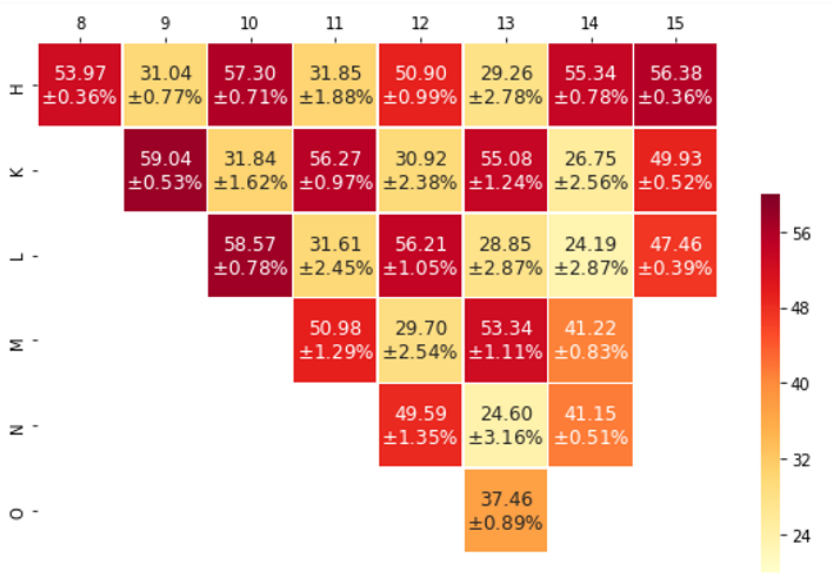

Figure 4.17 Burnups at EOC with Associated Uncertainties with consideration of NK-FM-TH correlations.

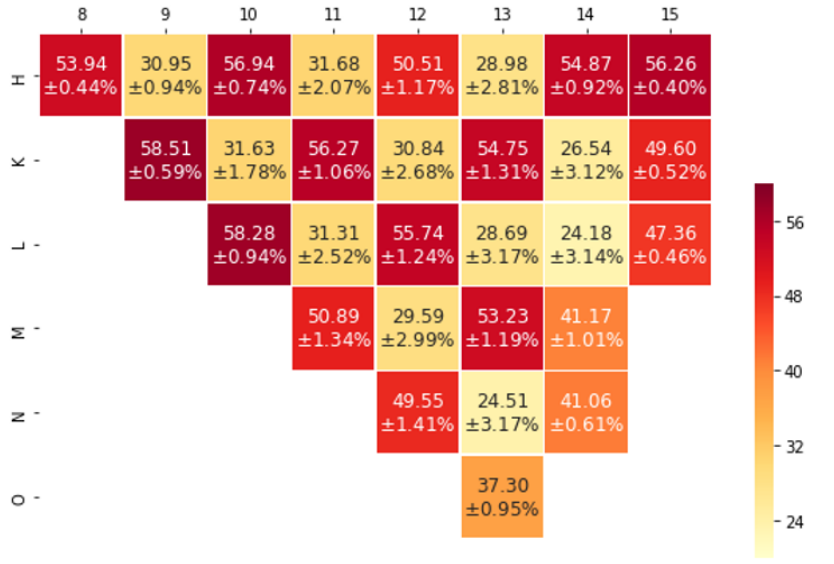

Figure 4.18 Burnups at EOC with Associated Uncertainties without consideration of NK-FM-TH correlations.

4.7 Summary

This Chapter demonstrates the uncertainty analysis of the TMI-1 core multi-physics simulations, including steady state simulation, control rod ejection transient and cycle depletion calculations. The input uncertainties considered includes nuclear data uncertainties and geometrical manufacturing uncertainties, whose uncertainties are propagated into few-group constants (NK), gap conductance (FM) and parameters related to thermal-hydraulics modelling (TH). A global VCM can be generated to represent the correlation between different physics domains. The final core output responses are calculated with associated uncertainties. By taking into consideration of the NK-FM-TH correlations, the uncertainties of core output responses are reduced. For example, the prediction of the 95% peak fuel temperature at BOC during control rod ejection accident is reduced by 37 K by considering the correlations.

By separately perturbing each of the input parameters, the total uncertainty of the core multi-physics simulation can be decomposed and the uncertainty contribution due to different input parameters can be evaluated. NK few-group constants are found to be the most influential uncertainty contributors in both steady state and transient simulations. A large uncertainty contribution from NK few-group constants are observed (0.5% Δk/k), which are partially due to the large measurement uncertainties of nuclear data.

CHAPTER

5

CONCLUSIONS AND FUTURE WORK

5.1 Conclusions

In this work, an innovative method for consistently propagating and quantifying uncertainties for the multi-physics PWR core simulation is developed based on stochastic sampling approach and demonstrated on the PWR benchmark problems.

The technical approach to represent the correlations between input parameters involve the usage of the global variance-covariance matrix (VCM) covering the NK few-group constants, FM and TH parameters. The sampling approach is used in constructing the global VCM. The correlated uncertainties of input parameters from different physics domains to performance and safety parameters are propagated through core multi-physics simulations by re-sampling the global VCM.

The framework is firstly demonstrated in the PWR mini-core problem. The geometrical manufacturing uncertainties are considered and propagated into few-group constants, gap conductance and parameters related to TH model. By taking into account different correlations into account when sampling step of the global VCM, the impact of NK-FM, NK-TH, and NK-FM-TH correlations on core multi-physics steady state and transient simulations are studied. It is observed that the uncertainties of core outputs tends to be smaller when correlations are taken into account. For example, the uncertainty of peak fuel temperature at BOC during control rod ejection accident is 37 K smaller at BOC with the consideration of correlations than otherwise.

This consistent uncertainty analysis framework is further implemented in the uncertainty analysis of the TMI-1 core simulation. In the steady state calculations, the uncertainty for the core k_{eff} is found to be less than 0.6% and mainly contributed by the nuclear data. The normality test suggests that the core k_{eff} and power peaking factors can both be described by a normal distribution. The confidence intervals of core outputs are also computed and summarized. Time evolution of core reactivity, power, and peak fuel temperature as a result of an ejected control rod are also studied. Moreover, cycle depletion analysis is also performed and the uncertainties of assembly burnup is calculated. It is observed that the uncertainties of core output responses are decreased with consideration of the multi-physics correlations, which indicates that the safety margin is increased with consideration of the correlations.

The major contribution of this Ph.D. work includes the development of the framework for consistent uncertainty propagation and quantification. It is also important to realize that the correlations between input parameters are important and non-negligible. The uncertainty quantification results suggest that the prediction of uncertainties of core outputs tends to be smaller when correlations are taken into account for both PWR mini-core and TMI-1 problems.

5.2 Future Work

Although the main findings of this work is favourable, there are multiple aspects that can be done to improve the quality of this work. The major limitation of this work stems from the fact that only the geometrical manufacturing uncertainties and nuclear data uncertainties are considered, while there are many other important sources of input uncertainties were left out. For example, uncertainties related to fuel composition and fuel density during fuel rod fabrication are also important, and are expected to have impact on both fuel conductivity (for FM) and few group constants (for NK) simulation. In the future, a more detailed modeling using fuel rod modeling code (e.g. FRAPCON/FRAPTRAN) is recommended to evaluate the impact of fuel manufacturing uncertainties on fuel properties. The correlations between few-group constants and fuel properties due to fuel density and compositions uncertainties will need to be evaluated, and consistently propagated through core multi-physics simulation.

The work can also be improved by performing a more efficient sampling of the VCM. As demonstrated in Figure 3.6, the dimension of global VCM is large due to the fact that the few-group constants are generated at different data points of fuel temperature, moderator density, boron concentration, control rod insertion status and burnups. For large PWR core such as TMI-1 reactor core, this global VCM is even larger because there are 11 different types of fuel assemblies. The few-group constants related to different types of assemblies also needs to be considered, which further expands the size of VCM by 11 times. However, the few-group constants are highly linear between each other, which provides the potential possibility of reducing the size of the global VCM while maintaining the accurate representation of the correlations. The principle component analysis (PCA) of the global VCM is suggested in the future to reduce the dimension of the matrix.

It is also worthwhile to mention that only a limited number of input uncertain parameters are considered in this work. There are other sources of input uncertainties, including

fuel conductivity, cladding conductivity from the fuel modelling space, and other TH related uncertain inputs such as heat transfer coefficient, core inlet temperatures, etc. The Appendix A provides a summary of previous studies aiming to investigate the impact of some of these influential input parameters without considering their correlations. It is suggested to perform a global sensitivity analysis to identify more influential parameters, and investigate their impact on uncertainties of core multi-physics simulations using the consistent uncertainty propagation framework proposed in this work.

BIBLIOGRAPHY

[1] U.S.NRC. *10 CFR Part 50 - Definitions*. URL: https://www.nrc.gov/reading-rm/doc-collections/cfr/part050/part050-0002.html.

[2] Boyack, B. et al. "Quantifying Reactor Safety Margins Part 1: An Overview of the Code Scaling, Applicability, and Uncertainty Evaluation Methodology". *Nuclear Engineering and Design* **119** (1990), pp. 1–15.

[3] Wilson, G. et al. "Quantifying Reactor Safety Margins Part 2: Characterization of Important Contributors to Uncertainty". *Nuclear Engineering and Design* **119** (1990), pp. 17–31.

[4] Wulff, W. et al. "Quantifying Reactor Safety Margins Part 3: Assessment and Ranging of Parameters". *Nuclear Engineering and Design* **119** (1990), pp. 33–65.

[5] Lellouche, G. et al. "Quantifying Reactor Safety Margins Part 4: Uncertainty Evaluation of LBLOCA Analysis Based on Trac-PF1/Mod 1". *Nuclear Engineering and Design* **119** (1990), pp. 67–95.

[6] Zuber, N. et al. "Quantifying Reactor Safety Margins Part 5: Evaluation of Scale-Up Capabilities of Best Estimate Codes". *Nuclear Engineering and Design* **119** (1990), pp. 97–107.

[7] Catton, I. et al. "Quantifying Reactor Safety Margins Part 6: A Physically Based Method of Estimating PWR Large Break Loss of Coolant Accident PCT". *Nuclear Engineering and Design* **119** (1990), pp. 109–117.

[8] Glaeser, H. "Evaluation of Licensing Margins of Operating Reactors Using 'Best Estimate Methods Including Uncertainty Analysis". *5th Seminar on Scaling Uncertainty and 3D Coupled Code Calculations in Nuclear Technology* (2006).

[9] Rohatgi. *Historical perspectives of BEPU research in United States*. Brookhaven National Laboratory, 2018.

[10] Ivanov, K. et al. "Uncertainty Analysis in Reactor Physics Modeling". *Science and Technology of Nuclear Installations* **2013** (2013), pp. 1–2.

[11] Ivanov, K. et al. *Benchmarks for Uncertainty Analysis in Modelling (UAM) for the Design, Operation and Safety Analysis of LWRs. Volume I: Specification and Support Data for Neutronics Cases (Phase I)*. OECD NEA, 2013.

[12] Hou, J. et al. *Benchmarks for Uncertainty Analysis in Modelling (UAM) for the Design, Operation and Safety Analysis of LWRs. Volume III: Specification and Support Data for the System Cases (Phase III)*. OECD NEA, 2013.

[13] Wieselquist, W. et al. “PSI Methodologies for Nuclear Data Uncertainty Propagation with CASMO-5M and MCNPX: Results for OECD/NEA UAM Benchmark Phase I”. *Nuclear Engineering and Design* **2013** (2013), pp. 1–15.

[14] Zeng, K. et al. “Uncertainty Analysis of Light Water Reactor Core Simulations Using Statistic Sampling Method”. *MC 2017* (2017).

[15] Hou, J. et al. “Comparative Analysis of Solutions of Neutronics Exercises of the LWR UAM Benchmark”. *MC 2019* (2019).

[16] Porter, N. et al. “Uncertainty Quantification Study of CTF for the OECD/NEA LWR Uncertainty Analysis in Modeling Benchmark”. *Nuclear Science and Engineering* **192** (2018), pp. 271–286.

[17] Radaideh, M. et al. “Sampling-based Uncertainty Quantification of the Six-group Kinetic Parameters”. *Reactor Physics Paving the Way Towards More Efficient Systems* (2018).

[18] Zeng, K. et al. “Uncertainty Quantification and Propagation of Multiphysics Simulation of the Pressurized Water Reactor Core”. *Nuclear Technology* **205** (2019), pp. 1618–1637.

[19] Delipei, G. “Multi-Physics Uncertainty Propagation in a PWR Rod Ejection Accident Modeling - Analysis Methodology and First Results”. *BEPU2018* (2018).

[20] Zeng, K. et al. “Impact of Spatial Coupling Schemes and Perturbation Options on Uncertainty Quantification of PWR Core Simulation”. *MC 2019* (2019).

[21] Yankow, A. “A Two-Step Approach to Uncertainty Quantification of Core Simulators”. *Science and Technology of Nuclear Installations* **2012** (1954), pp. 765–769.

[22] Anderson, T. “A Test of Goodness of Fit”. *Journal of the American Statistical Association* **49** (2012), pp. 1–9.

[23] Henderson, K. “Testing Experimental Data for Univariate Normality”. *Clinica Chimica Acta* **366** (2006), pp. 112–129.

[24] Downar, T. et al. *PARCS v3.0 U.S. NRC Core Neutronics Simulator User Manual*. University of Michigan, 2012.

[25] Bajorek, S. et al. *TRACE V5.0 Patch 5 User’s Manual*. U. S. Nuclear Regulatory Commission, 2016.

[26] Jessee, M. et al. “Polaris: a New Two-Dimensional Lattice Physics Analysis Capability for the SCALE Code System”. *Physor 2014* (2014).

[27] Readen, B. et al. *SCALE Code System*. Ork Ridge National Laboratory, 2016.

[28] Ivanov, K. et al. *Pressureised Water Reactor Main Stream Line Break (MSLB) Benchmark, Volume I: Final Specifications*. OECD Nuclear Energy Agency, 1999.

[29] Todorova, N. et al. "PWR REA Sensitivity Analysis of TRAC-PF1/NEM Coupling Schemes". *Ninth International Conference on Nuclear Engineering* (2001).

[30] Wysocki, A. et al. "The Modeling of Advanced Fuel Designs with the NRC Fuel Depletion Codes PARCS/PATHS". *Nuclear technology* **190** (2015), pp. 323–335.

[31] Adams, B. et al. *Dakota, A Multilevel Parallel Object-Oriented Framework for Design Optimization, Parameter Estimation, Uncertainty Quantification, and Sensitivity Analysis: Version 6.11 User's Manual*. Sandia National Laboratories, 2019.

[32] Wilks, S. "Determination of Sample Sizes for Setting Tolerance Limits". *The Annals of Mathematical Statistics* **12** (1941).

[33] Hong, S. *Generic Application of Wilks' Tolerance Limit Evaluation Approach to Nuclear Safety*. OECD NEA, 2013.

APPENDIX

APPENDIX

A

IMPACT OF SPATIAL COUPLING SCHEMES AND PERTRUBATION OPTIONS ON UNCERTAINTY QUANTIFICATION OF PWR CORE SIMULATION

The study described in this Appendix performs the uncertainty quantification on PWR core performance at both steady state and asymmetric rod ejection accident (REA) transient, with a focus on evaluating the impact of different perturbation options and spatial

coupling schemes (mesh overlays) on core multi-physics simulation. The input uncertainty of the neutronics simulation includes nuclear data uncertainty propagated through few-group cross sections and kinetics parameters. Several heat transfer related parameters for fuel modeling are considered as sources of input uncertainty of the thermal-hydraulics simulation using TRACE, including the thermal conductivity of the fuel and cladding, and gap conductance. DAKOTA is used for performing the stochastic sampling of input parameters, driving the TRACE/PARCS coupled calculations, and evaluating the uncertainties of core responses. The uncertainty quantifications with different neutron-kinetics/thermal-hydraulics (NK-TH) coupling schemes are analyzed in this paper, including the one-dimensional Channel model and three-dimensional Cartesian model. The input uncertainties are perturbed independently in each physics domain, but the spatial correlations are varied: the input parameters could be perturbed based on reactor core, different thermal hydraulics channels or fuel assemblies. The impact of those different perturbation options is evaluated in the Appendix. Several mesh refinement analyses on the PWR modeling has been performed previously. The PWR REA mesh sensitivity analysis was performed with the use of various coupling schemes using TRAC-PF1/NEM [29], which reveals that it is necessary to represent each fuel assembly by one heat structure. The NRC investigated the use of different thermal-hydraulics models on predicting safety limits of APR1400 reactor with TRACE/PARCS [25]. Observable deviations in core simulation results were found with the use of different coupling schemes or models, and the use of finer meshes and spatial overlays is recommended. These studies mostly focus on model verification and comparison, while the influence of different spatial coupling schemes on core uncertainty evaluation remains to be investigated. This work focues on evaluating the impact of the use of refining meshes on PWR core uncertainty quantification and investigating the uncertainty propagation with different perturbation options, i.e., perturbing input parameters based on reactor core, thermal-hydraulics channels or fuel assemblies.

A.1 Coupling Schemes

The first coupling scheme studied in this paper was initially developed for the main steam line break benchmark in and named as 1-D Channel model. The reactor core was represented with 19 parallel vertical PIPE components (TH channels), where each PIPE represents one TH channel consisted of several fuel assemblies or radial reflector region, as shown in Figure A.1 (b). One-dimensional TH calculation was performed with given pre-calculated mass flow rate for each channel, and no cross flow between channels were taken into account. Generally, each of the fuel assemblies was represented by its own heat structure component (HTSTR), except those located on the central row, where one assembly was split into two HTSTRs due to TH modeling decision. Axially, four neutron-kinetics (NK) nodes were linked to one TH and HTSTR cells in an aligned manner. Figure A.1 (c) depicts the radial overlays of the second coupling scheme investigated in this study, which was built in Cartesian geometry using VESSEL component with an accurate representation of the square-pitched reactor core and thus has the capability of calculating 3-dimensional flow field. Similarly, the core was discretized radially into 193 HTSTR, which allows a one-to-one mapping among TH cells, heat conduction elements and the neutronics assemblies (TH-HTSTR-NK). The axial nodalization and TH-HTSTR-NK mapping in Cartesian model remains the same as the Channel model, thus only the impact of radial coupling scheme was investigated in this study. In order to make a consistent comparison, the mass flow rate distribution was pre-calculated from the Cartesian model and used as fixed boundary conditions in the Channel model.

A.2 Input Uncertainties

Sampler, a stochastic sampling based capability in SCALE code package, is used to sample SCALE 56-group variance/covariance library, and the nuclear data uncertainty is prop-

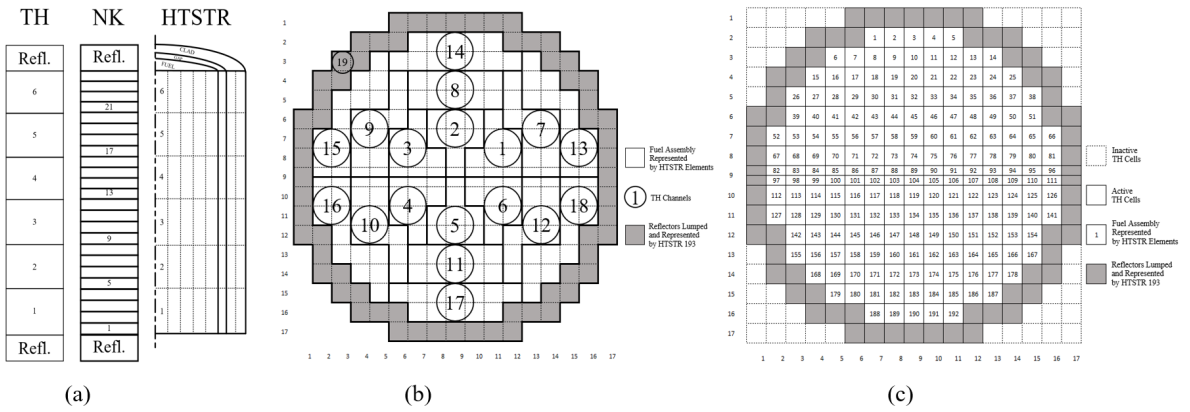

Figure A.1 Axial TH-HTSTR-NK Mapping(a), 1-D Channel Model (b), 3-D Cartesian Model (c).

agated through the two-group cross sections and six-group kinetic parameters through lattice calculation. Note that only nuclear cross sections are considered in the current study. DAKOTA [31] has been coupled with TRACE/PARCS for core multi-physics uncertainty quantification purposes. DAKOTA is capable of generating uncertain values for fuel modeling parameters according to user-defined probability distributions, invoking core simulation using TRACE/PARCS, and finally quantifying the uncertainty of output responses. A python interface has been developed for pairing one set of nuclear cross sections to a random set of perturbed fuel modeling parameters, as shown in Figure A.2. The nominal values of fuel modeling parameters can be found in [12], while the associated uncertainties are summarized in Table I.

The impact of different coupling schemes on core uncertainties can be quantified by inserting corresponding TH models in TRACE/PARCS calculation. For each perturbed core calculation, only one sample of input parameters is generated and assigned to the whole core. Besides that, this work also investigates the impact of different perturbation options. The core 3-D Cartesian model is selected for this investigation. The perturbation of nuclear data remains the same for different options by keeping the same cross sections assignment, while the fuel modeling parameters are perturbed based on the following three perturbation options and the uncertainties of output responses are compared: (1) Core-based: 1 sample

Table A.1 Summary of the geometrical manufacturing uncertainties considered for TMI-1 large-scale core problem.

Parameters	Distribution	Rel. Std.
Fuel Thermal Conductivity K_f	Normal	5.00 %
Cladding Thermal Conductivity K_c	Normal	5.00%
Fuel Heat Capacity C_p	Normal	5.00%
Gap Conductance H_{gap}	Uniform	25 %
Nuclear data uncertainty		ENDF/B-VII.1, SCALE 56-group VCM

of input parameters is generated and assigned to the whole core; (2) Channel-based: 18 samples of input parameters are generated, each assigned to 1 of the 18 fuel channels; (3) Assembly-based: 177 samples of input parameters are generated, each assigned to 1 of the 177 fuel assemblies.

The Wilks' theorem [32] [33] is applied in this study to determine the minimum number of computational samples required to achieve sufficient tolerance limit with a certain level of confidence. To establish 95% confidence of the 95% tolerance limits of core output responses, a minimum of N=93 sets of code executions are performed and the core responses are extracted and analyzed. The Anderson-Darling test is selected to assess the normality of the output responses with the so-called A^2 value, which measures the average deviation of the distribution of output response from a perfect normal distribution. A computed A^2 value that is greater than the threshold value of 0.757 rejects the assumption that the output response is normally distributed. Once the output response is quantified as normally distributed, the confidence interval of the true uncertainty (a.k.a. 'the uncertainty of true uncertainty') can be calculated as [88%σ, 116%σ] under sample size of 93, where σ is the uncertainty computed from 93 samples.

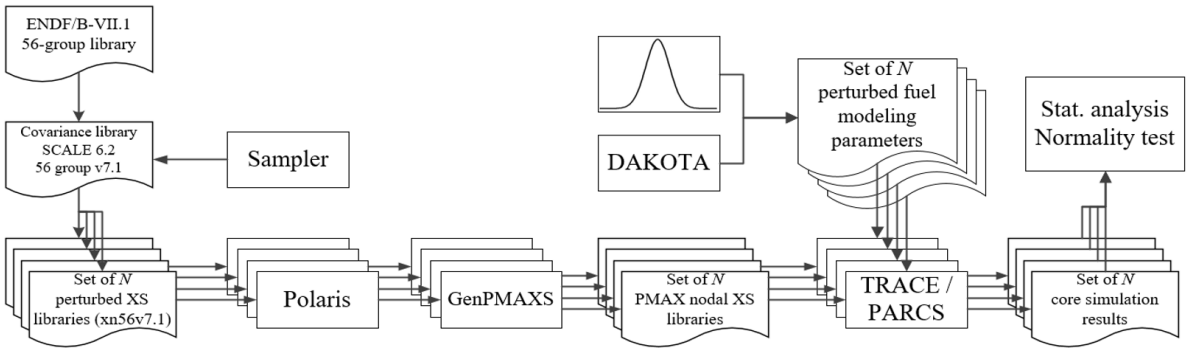

Figure A.2 PWR Core Uncertainty Quantification with Stochastic Sampling Method.

A.3 Impact of Spatial Coupling Schemes on Core Uncertainty Quantification

The mass flow rate computed by Cartesian model at different TH cells may vary between samples due to the perturbation of input parameters. Figure A.3 presents the coolant mass flow rate with associated uncertainties using Cartesian model at steady state and transient conditions, respectively. For the Channel model, the mass flow rate for each channel is obtained by homogenizing assembly mass flow rates in Cartesian model, and used as fixed inlet boundary condition without uncertainty. This introduces additional uncertainty compared when Cartesian model is used, and this uncertainty is less than 0.10% at steady state while can be as large as 0.13% during the transient. Note that with Cartesian model, the local coolant mass flow rate around the hot spot location increase from 88 kg/s at steady state into 91 kg/s at the end of transient, and thus helps to reduce peak fuel and coolant temperatures.

Core simulations are performed using the Channel and Cartesian models separately. Table II summarizes the simulation results at nominal state, including core multiplication factor keff, radial power peaking factor F_R and axial power peaking factor F_z at steady state (S.S.), and maximum reactivity insertion ρ^{max}, core total power P^{max} and fuel temperature

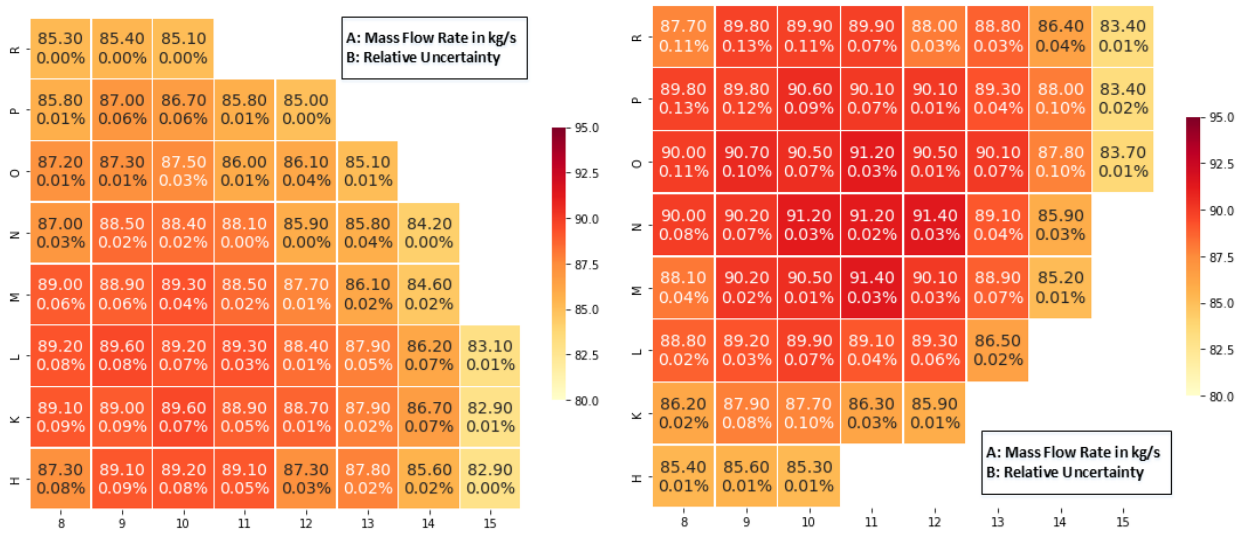

Figure A.1 Uncertainties of Assembly Mass Flow Rate with Cartesian Model at SS (left) and TR (right) Conditions.

T_f^{max} during REA transient (TR). The 3-D TH calculation and coolant mixing of different TH cells help to decrease the fuel and coolant temperatures, and thus improve neutron thermalization and yield higher fission rate. Therefore, Cartesian model tends to predict higher SS k_{eff}, TR ρ^{max} and P^{max}. The TR T_f^{max} is more complex and affected by two antagonistic effects. On the one hand, the use of Cartesian model predicts a larger P^{max} which increases T_f^{max}; on the other hand, enabling the 3-D coolant mixing increase local mass flow rate at hot spot and thus decreases T_f^{max}. It is found that the peak fuel temperature is brought down from 2737 K to 2606 K at BOC with the use of Cartesian model, even though a larger P^{max} (4%) is observed. However, the P^{max} at EOC predicted with Cartesian model is 17% larger than that from Channel model and the first effect becomes dominant, resulting in a 103 K higher peak fuel temperature.

Table A.2 summarizes the simulation results at nominal state, including core multiplication factor k_{eff}, radial power peaking factor F_{R} and axial power peaking factor F_{Z} at steady state (SS),

and maximum reactivity insertion ρ^{max}, core power P^{max} and fuel temperature T_f^{max} during REA transient (TR). The 3-D TH calculation and coolant mixing of different TH cells help to decrease the fuel and coolant temperatures, and thus improve neutron thermalization and yield higher fission rate. Therefore, Cartesian model tends to predict higher SS k_{eff}, TR ρ^{max} and P^{max}. The TR T_f^{max} is more complex and affected by two antagonistic effects. On the one hand, the use of Cartesian model predicts a larger P^{max} which increases T_f^{max}; on the other hand, enabling the 3-D coolant mixing increase local mass flow rate at hot spot and thus decreases T_f^{max}. It is found that the peak fuel temperature is brought down from 2737 K to 2606 K at BOC with the use of Cartesian model, even though a larger P^{max} (4%) is observed. However, the P^{max} at EOC predicted with Cartesian model is 17% larger than that from Channel model and the first effect becomes dominant, resulting in a 103 K higher peak fuel temperature.

Table A.2 Core Responses at Nominal State in Steady State and Transient Simulations.

Condition / Core Responses / Model	HFP BOC			HFP EOC		
	SS k_{eff}	SS F_R	SS F_z	SS k_{eff}	SS F_R	SS F_z
1-D Channel Model	1.01501	1.349	1.315	0.98290	1.402	1.190
3-D Cartesian Model	1.01848	1.395	1.396	0.98597	1.433	1.152
	TR ρ^{max} (\$)	TR P^{max}	TR T_f^{max} (K)	TR ρ^{max} (\$)	TR P^{max}	TR T_f^{max} (K)
1-D Channel Model	0.39	1.66	2737	0.36	1.59	1869
3-D Cartesian Model	0.40	1.70	2606	0.42	1.76	1972

Table A.3 summarizes the mean value of core output responses with associated uncertainties computed from 93 random samples at steady state. The multi-physics uncertainty is first quantified, and further breakdown into single physics, as presented by different rows of Table A.3.

Very close uncertainty in core k_{eff} is observed from different models, and the uncertainty is mostly contributed by nuclear data. The use of Cartesian model only introduces less than 0.10% of input uncertainty in mass flow rate, which is very small and does not reflect a large impact on the uncertainty of core k_{eff}.

Table A.3 Uncertainty Quantification of Core Steady State Simulations.

Source of uncertainty	State	Sample SS k_{eff} ± Rel. σ		Sample SS F_z ± Rel. σ		Sample SS F_R ± Rel. σ	
		1-D Channel Model	3-D Cartesian Model	1-D Channel Model	3-D Cartesian Model	1-D Channel Model	3-D Cartesian Model
All	BOC	1.01501 ±0.47%	1.01848 ±0.47%	1.315 **±0.47%**	1.397 ±0.20%	1.348 ±0.62%	1.395 **±0.81%**
	EOC	0.98295 ±0.45%	0.98798 ±0.44%	1.190 ±0.65%	1.156 **±0.84%**	1.409 ±0.77%	1.435 **±0.95%**
Nuclear Data only	BOC	1.01507 ±0.46%	1.01852 ±0.46%	1.315 **±0.33%**	1.397 ±0.20%	1.348 ±0.61%	1.395 **±0.81%**
	EOC	0.98298 ±0.44%	0.98800 ±0.44%	1.190 ±0.64%	1.156 **±0.84%**	1.409 ±0.77%	1.435 **±0.96%**
Fuel Modeling parameters only	BOC	1.01472 ±0.05%	1.01843 ±0.03%	1.314 **±0.32%**	1.396 ±0.05%	1.346 ±0.08%	1.395 **±0.15%**
	EOC	0.98287 ±0.03%	0.98790 ±0.03%	1.190 **±0.18%**	1.156 ±0.04%	1.402 ±0.03%	1.435 ±0.03%

The uncertainties of F_z and F_R are evaluated by directly extracting the maximum relative assembly power regardless the peaking location. As shown in Figure A.2 and Figure A.3, the use

of Cartesian model greatly changes the axial power profiles and radial power distributions, and finally affects the evaluations of uncertainties because flatter power profile can potentially increase the uncertainties of power peaking factors. For example, a significant difference can be observed in the uncertainty of F_z between two models. Channel model predicts larger uncertainty of F_z at BOC, which is partially attributed to the shift of axial power peaking locations. As shown in Figure A.2, F_z is found to be located at the 12th node for all of the samples in Cartesian prediction, while the Channel model tends to predict a flatter axial power profile at BOC and the locations of F_z shift between the 11th (33% of the samples) node and 12th (67% of the samples) node. The same analysis applies to the larger uncertainty of F_z predicted with Cartesian model at EOC, where a flatter axial power profile was observed as shown in Figure A.2.

As shown in Table A.3, both models consistently predict larger uncertainty in F_R at EOC than that at BOC. The radial power distribution becomes flatter due to burn-up at EOC, and therefore, the uncertainty increases due to the more frequent changes of assembly peaking locations. Figure A.3 depicts the radial power distribution at BOC. It is found that the Cartesian model tends to predict a larger uncertainty in assembly power. The use of Cartesian model provides coolant mixing and calculates local mass flow rate for each assembly, while the Channel model only provides fixed mass flow rate to assemblies located in the same channel and no cross flow is considered. The 3-D coolant mixing effect tends to reduce coolant and fuel temperatures, increasing the local neutron thermalization, which finally increases the radial power peaking factor. As shown in Figure A.3, the uncertainty of assembly power predicted with Cartesian model is found to be slightly larger, which can be explained by the additional uncertainty in local mass flow rate. It is found that the peaking location also jumped between assembly L11 and K10 for

predictions of Cartesian model, which finally slightly increases the uncertainty of radial peaking factors from 0.70% to 0.81%.

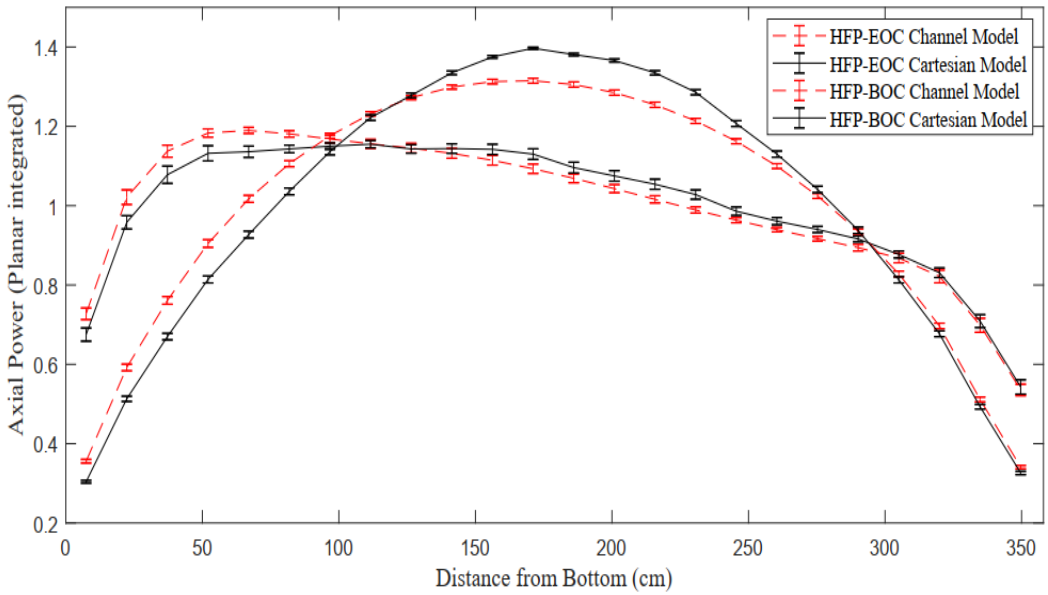

Figure A.2 Axial Power Profile at BOC (left) and EOC (right), Predicted with Channel Model (blue) and Cartesian Model (red).

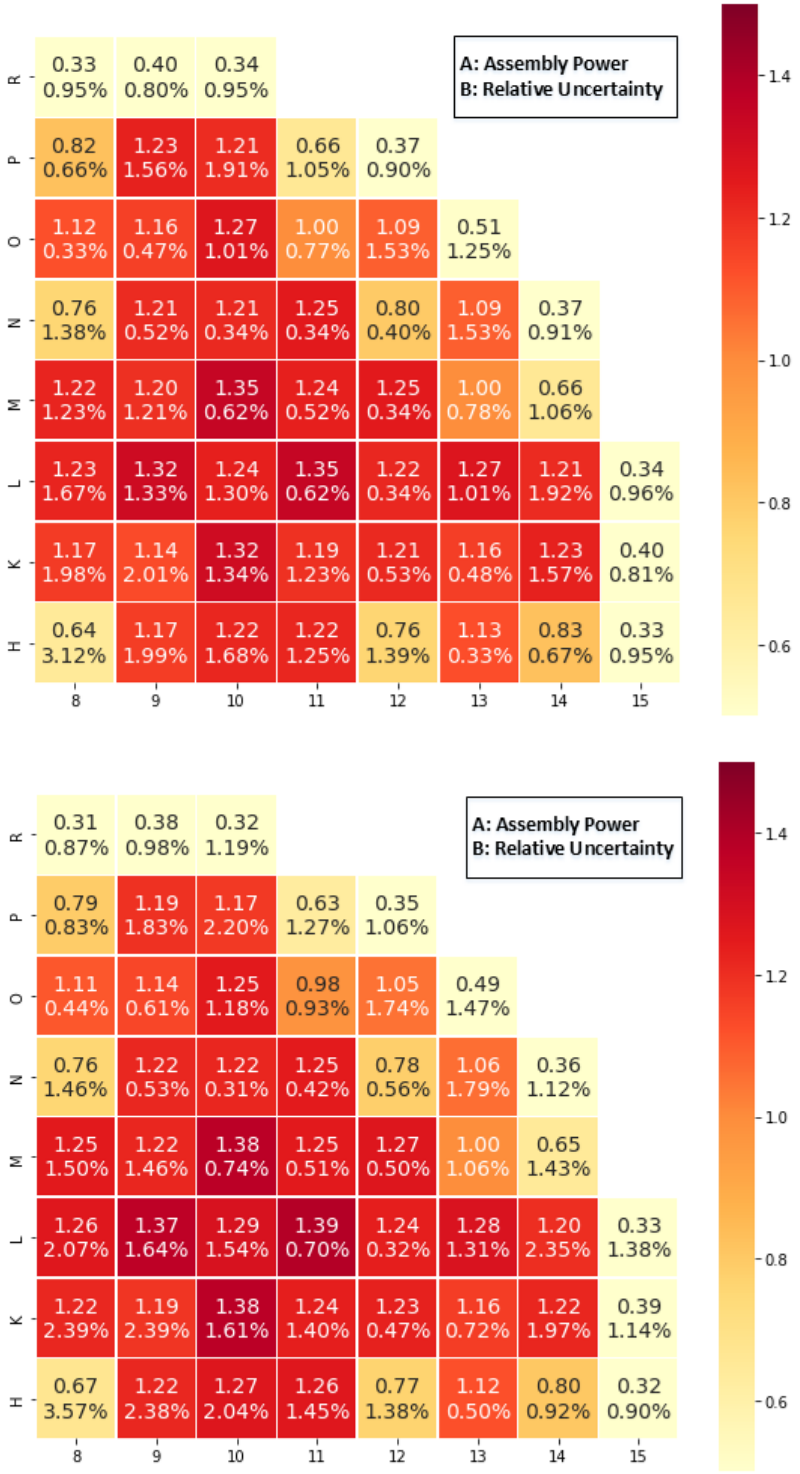

Figure A.3 Radial Power Distribution at BOC, Predicted with Channel Model (top) and Cartesian Model (bottom).

Anderson-Darling normality test is performed to quantify the distribution of core output responses, as shown in Table A.4. Note that the peaking location of F_Z and F_R may vary from sample to sample and there are two methods in reporting the radial power peaking factors. In the first method (denoted as M1), the peaking factor is extracted from maximum relative power taken from the core results regardless the peaking location. In the second method (M2), the peak location is identified first based on the mean power distribution over all samples, and the associated uncertainty is calculated. Generally, the A^2 value is found to be larger in output responses predicted with Cartesian model, implying that the use of 3-D TH calculation tends to drive the output responses away from a normal distribution. Due to the possible change in peaking location, the uncertainty estimated with M2 tends to be smaller than M1. It is found that core k_{eff} and F_z computed with Cartesian model follows a normal distribution by having an A^2 value smaller than the threshold of 0.757. The deviation from normal distribution is also found to be larger when M1 is employed. For example, normality is rejected in the distribution of F_R predicted using Cartesian model with M1 method because radial power peaks at assemblies located L11 and K10 among different samples, while the power peaking factor extracted with M2 approach passes normality test. The confidence intervals can be evaluated as [88%σ, 116%σ] for normally distributed parameters. For example, the confidence interval of the core k_{eff} predicted by Cartesian model at BOC is determined as [0.41%, 0.55%].

Table A.4 Anderson-Darling Normality Test of Core Steady State Simulations.

State	Methods	A^2 of k_{eff}		A^2 of F_z		A^2 of F_R	
		1-D Channel Model	3-D Cartesian Model	1-D Channel Model	3-D Cartesian Model	1-D Channel Model	3-D Cartesian Model
BOC	M1	0.692	0.736	0.291	0.685	0.303	**1.112 (FAIL)**
	M2	N/A	N/A	0.195	0.301	0.233	0.560
EOC	M1	0.575	0.599	0.476	0.324	0.327	0.402
	M2	N/A	N/A	0.321	0.233	0.305	0.454

Figure A.4 depicts the time evolution of ρ^{max}, P^{max}, and T_f^{max} computed with two models. It could be found that the uncertainties of ρ^{max} and P^{max} are mostly contributed by nuclear data, and the time evolution behaviors of these two outputs predicted from different models are very similar. For example, the largest and smallest reactivity insertions were observed in the 34th and 49th sample, using both models, respectively.

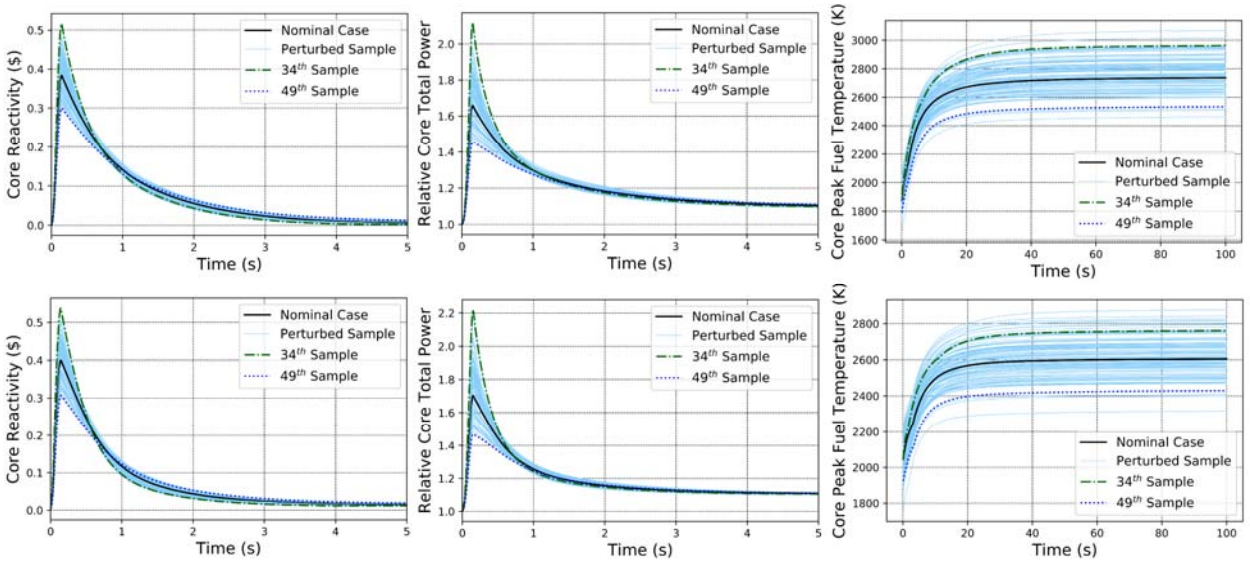

Figure A.4 Time Evolution of $\boldsymbol{\rho^{max}}$, $\boldsymbol{P^{max}}$, and $\boldsymbol{T_f^{max}}$ Predicted with Channel Model (top) and Cartesian Model (bottom).

Table A.5 presents the peak reactivity insertion, peak power, and peak fuel temperature during the REA transient. Larger uncertainties in ρ^{max} and P^{max} are observed with the use of Cartesian model, because additional uncertainty (less than 0.16%) is introduced by mass flow rate during transient. Compared to Channel model, Cartesian model predicts a lower mean value of T_f^{max} at BOC due to coolant mixing, and higher mean value of T_f^{max} at EOC because larger transient power is inserted. Comparing the uncertainty of T_f^{max}, it can be found that the additional uncertainty in mass flow rate increases the uncertainty of T_f^{max} when only uncertainties from fuel modeling parameters are considered, while decreases the uncertainty of T_f^{max} when only nuclear data uncertainty is considered. This phenomenon implies that the correlations between nuclear data, fuel modeling parameters and thermal-hydraulics conditions are important in uncertainty evaluation of T_f^{max}.

Table A.5 Uncertainty Quantification of Core REA Transient Simulations.

Source of uncertainty	State	Sample ρ^{max} (\$) ± Rel. σ		Sample P^{max} ± Rel. σ		Sample T_f^{max} (K) ± Rel. σ	
		1-D Channel Model	3-D Cartesian Model	1-D Channel Model	3-D Cartesian Model	1-D Channel Model	3-D Cartesian Model
All	BOC	0.40±11.78%	0.41±**12.00%**	1.701±7.98%	1.740±**8.61%**	2765±**4.44%**	2620±4.19%
	EOC	0.37±15.31%	0.42±**15.66%**	1.640±9.60%	1.801±**12.34%**	1874±3.80%	2133±**3.91%**
Nuclear Data only	BOC	0.39±11.82%	0.41±**11.96%**	1.691±7.87%	1.740±**8.57%**	2634±**1.44%**	2609±1.08%
	EOC	0.37±15.30%	0.42±**15.60%**	1.624±9.35%	1.800±**12.27%**	1873±**0.84%**	2118±0.71%
Fuel Modeling parameters only	BOC	0.38±0.46%	0.40±**0.58%**	1.658±0.30%	1.692±**0.39%**	2749±3.88%	2614±**3.97%**
	EOC	0.36±0.41%	0.41±**0.69%**	1.589±0.24%	1.727±**0.48%**	1872±3.73%	2125±**3.86%**

A.4 Impact of Perturbation Options on Core Uncertainty Quantification

In addition to comparing the uncertainty quantification results obtained using different coupling schemes, this work also investigats the impact of the spatial correlation of input parameters. The fuel modeling parameters are perturbed with three options detailed in Section A.2, and applied into uncertainty quantification of core steady state and transient simulations using Cartesian model. The nuclear cross sections assignment remains the same for all three perturbation options, and only the impacts of perturbing fuel modeling parameters with different options are investigated.

As shown in Table A.6, the uncertainty of core SS k_{eff} and TR ρ^{max} remains very similar for all three perturbation options, because their uncertainty is mostly contributed by nuclear data, while fuel modeling parameters only have negligible influence. The last two rows of Table A.6 presents the results when only fuel modeling parameters are perturbed in different options. The mean values of F_{R} are found to be closed when different perturbation options are applied, basically because inputs are randomly sampled from the same normal distribution for all three perturbation options. The uncertainty of F_{R} contributed by fuel modeling parameters increases when the perturbation is applied in a finer mesh, implying the spatial correlation of fuel modeling parameters has a large impact on core single physics uncertainty quantification. However, the uncertainty of F_{R} is found to be similar for all three options when uncertainty from both nuclear data and fuel modeling parameters are considered, as shown in the first two rows. This may imply that the correlations between input parameters from different physics domains is more significant and overwhelms the impact of spatial correlations. Quantify the influence of correlations between

parameters form multi-physics domains is therefore important and will be investigated in the future.

Table A.6. Impact of Spatial Correlations on Core Uncertainty Quantification.

Source of Uncertainty	State	Core-based			Channel-based			Assembly-based		
		SS k_{eff}	SS F_R	TR ρ^{max}	k_{eff}	F_R	TR ρ^{max}	k_{eff}	F_R	TR ρ^{max}
All	BOC	1.01848 ±0.47%	1.395 **±0.81%**	0.41 ±12.00%	1.01848 ±0.46%	1.402 **±0.86%**	0.41 ±12.01%	1.01848 ±0.46%	1.402 **±0.84%**	0.41 ±12.10%
	EOC	0.98798 ±0.44%	1.435 **±0.95%**	0.42 ±15.66%	0.98650 ±0.44%	1.456 **±0.95%**	0.43 ±15.74%	0.98655 ±0.44%	1.450 **±0.91%**	0.43 ±15.80%
Nuclear Data only	BOC	1.01852 ±0.46%	1.395 ±0.81%	0.41 ±11.96%	1.01852 ±0.46%	1.395 ±0.81%	0.41 ±11.96%	1.01852 ±0.46%	1.395 ±0.81%	0.41 ±11.96%
	EOC	0.98800 ±0.44%	1.435 ±0.96%	0.42 ±15.60%	0.98800 ±0.44%	1.435 ±0.96%	0.42 ±15.60%	0.98800 ±0.44%	1.435 ±0.96%	0.42 ±15.60%
Fuel Modeling parameters only	BOC	1.01843 ±0.03%	1.395 **±0.15%**	0.40 ±0.58%	1.01843 ±0.02%	1.402 **±0.41%**	0.40 ±1.15%	1.01843 ±0.02%	1.402 **±0.45%**	0.40 ±1.23%
	EOC	0.98790 ±0.03%	1.435 **±0.03%**	0.41 ±0.69%	0.98642 ±0.02%	1.455 **±0.32%**	0.41 ±0.65%	0.98650 ±0.44%	1.455 **±0.98%**	0.41 ±0.68%

A.5 Summary

In this work, the TMI-1 core multi-physics simulation is performed by using different NK-TH-HTSTR coupling schemes, and the associated uncertainties of output responses are quantified in both steady state simulation and REA transient. It is found that different coupling schemes have negligible influence on uncertainty of core k_{eff}, but can significantly affect core power peaking

factors. The uncertainty of F_z and F_R tends to be larger when model predicts a flatter power distribution, which tends to enhance the change of location where peak power is observed. Generally, the use of 3-D Cartesian model tends to increase the uncertainties of steady state F_R, while at the same time drives the distribution of output responses away from normality. Compared with 1-D Channel model, the use of 3-D Cartesian model automatically introduce additional uncertainty in mass flow rate, and increases the uncertainty of transient ρ^{max} and P^{max}. Future work of this study will include investigation of the reactivity feedback components to reveal the local TH-NK feedback effect by using different coupling schemes.

The impact of spatial correlation of fuel modeling parameters on core uncertainty evaluation is also investigated. It is found that the spatial correlation of fuel modeling parameters has a significant impact on core uncertainty quantification of single physics. However, this impact is overwhelmed by nuclear data in core multi-physics uncertainty quantification. In the future, the impact of correlations between input parameters of different physical domains will be investigated and compared in detail.